Thermoreversible associating polymer networks. I. Interplay of thermodynamics, chemical kinetics, and polymer physics

Robert S. Hoy[1,a)] and Glenn H. Fredrickson[1,2]

[1]*Materials Research Laboratory, University of California, Santa Barbara, California 93106, USA*
[2]*Departments of Chemical Engineering and Materials, University of California, Santa Barbara, California 93106, USA*

Hybrid molecular dynamics/Monte Carlo simulations are used to study melts of unentangled, thermoreversibly associating supramolecular polymers. In this first of a series of papers, we describe and validate a model that is effective in separating the effects of thermodynamics and chemical kinetics on the dynamics and mechanics of these systems, and is extensible to arbitrarily nonequilibrium situations and nonlinear mechanical properties. We examine the model's quiescent (and heterogeneous) dynamics, nonequilibrium chemical dynamics, and mechanical properties. Many of our results may be understood in terms of the crossover from diffusion-limited to kinetically limited sticky bond recombination, which both influences and is influenced by polymer physics, i.e., the connectivity of the parent chains. © *2009 American Institute of Physics*. [doi:10.1063/1.3268777]

I. INTRODUCTION

Flexible synthetic polymers have long been of fundamental scientific interest because many of their properties arise from a few universal features such as the topological connectivity, random-walk-like structure, and excluded volume of the chain molecules. Less universal are the various attractive, "associative" intermolecular interactions[1,2] ranging from weak dispersion forces to strong covalent chemical bonds (in chemically crosslinked systems). Examples include hydrogen bonding, electrostatic attractions, and effective attractions driven by incompatibility with a solvent. These interactions lead to formation of supramolecular structures ranging from micelles to network gels.

Associating polymers (APs) differ from simple homopolymers in that chains contain a (typically fairly low) fraction of "sticky" monomers, which are different from the majority-species monomers. The sticky monomers form "sticky" bonds with each other via associative interactions weaker than permanent covalent bonds. These lead to formation of supramolecular aggregates. Unlike the closely related "living" or "equilibrium" polymers, the degree of polymerization of AP parent chains is fixed (in time) by permanent covalent backbone bonds.

The lifetime of the sticky bonds is finite. Depending on the nature of the associative interactions and ambient conditions (e.g., temperature, concentration), the supramolecular topology may be practically permanent, in which case the system forms a "chemical gel" (i.e., a crosslinked rubber), or so short-lived that the system is indistinguishable from a simple polymer solution, melt or glass. Between these limits, when the topology of the associated supramolecular aggre-

gates changes on a time scale comparable to the experiment, these systems form complex fluids with fascinating dynamical and mechanical properties.[3]

At fixed ambient conditions, the time scales for topological changes in AP systems are in principle set by three independent factors: the (a) thermodynamics (i.e., energetic strength relative to $k_B T$), (b) the chemical kinetics of the sticky bonds, and (c) the underlying nonassociative polymer physics. Thermodynamics set static quantities such as the size of the supramolecular aggregates and hence the position of the system relative to the percolative gelation transition. Kinetics set relaxation times through their effect on the rates of formation and breaking of sticky bonds. Polymer physics alters the dynamics through such effects as the random-walklike structure and uncrossability of chains, which give rise to the systems' underlying Rouse or reptation dynamics.[4] The interplay of (a)–(c) allows for the design of materials with exquisitely tunable rheological response. For this reason, APs have been the focus of intense experimental and theoretical study over the past two decades; see Refs. 2, 3, and 5–7 for reviews.

Changes in ambient conditions lead to thermoreversible property changes unique to AP systems, e.g., extremely sharply decreasing viscosity upon decreasing concentration or increasing temperature. These changes can be tuned (engineered), so APs have great potential as "smart" materials[2,3,6,8,9] in which the change in lifetime or concentration of the sticky bonds with ambient conditions leads to useful products. Applications include temperature-sensitive adhesives, coatings for heat-sensitive materials, and generally enhanced melt processability relative to conventional polymers.[8]

Static thermodynamic properties of AP systems, in particular the percolative gelation transition and local structural changes arising from associative interactions, have been ex-

---

a)Electronic mail: robert.hoy@yale.edu.

tensively studied. Analytic theories provide a good understanding of homogenous systems, and emerging numerical techniques such as self-consistent field theoretic simulations[10] and reaction-ensemble DPD[11] show promise for investigating inhomogeneous systems.

However, the dynamical, mechanical, and nonequilibrium properties of AP gels and networks remain poorly understood. Time dependent properties obviously depend on kinetics, and in addition to being of fundamental scientific interest, a better understanding of them may prove important in developing new applications of AP systems such as self healing materials.[9] The situation becomes particularly complex when the lifetime of the sticky bonds is not long or short compared to the "polymeric" relaxation times; this regime has been studied rather extensively for linear equilibrium polymers (see, e.g., Refs. [12]–[16]), but much less so for networks.

Analytic and quasianalytic approaches to AP dynamics and mechanics, e.g.,[17] Refs. [7] and [18]–[30], have made many useful, experimentally verifiable predictions, including nonlinear behaviors such as shear thickening and strain hardening.[30,31] In the general case, however, the complex interplay of sticky bond thermodynamics and kinetics with the underlying polymer physics in these systems is almost certainly beyond the reach of analytic theory. For the sake of tractability, theories have generally neglected one or more features of AP systems that are likely essential to capturing their behavior under certain ambient conditions. For example, as temperature drops towards the glass transition, attractive, nonassociative interactions, such as van der Waals forces between nonsticky monomers, become increasingly important.[32] Moreover, virtually all analytic treatments have thus far been restricted[33] to homogeneous AP systems; the majority focus on the "telechelic" case of APs with only 2 sticky monomers per parent chain (one on each end). We believe that inhomogeneous AP systems are potentially the most interesting and useful, e.g., because inhomogeneities serve to localize sticky monomer (SM) concentration and network connectivity, which in turn can broaden the relaxation spectrum.[34,35]

The above set of potentially essential features of APs is not treated microscopically by existing theories, but can be readily captured by particle-based simulations. This is the first of a series of simulation studies, the goal of which is to elucidate the separate effects of sticky bond (SB) thermodynamics, kinetics, and other underlying polymer physics on the dynamical, mechanical, and nonequilibrium properties of APs.

Previous particle-based simulations of AP networks focusing on dynamical properties, e.g.,[17] Refs. [36]–[47] have produced a wealth of interesting ideas and results. However, for various reasons outlined in Sec. II B, the methods employed in these previous studies are not suitable for the full range of problems we wish to consider. A more versatile model for APs requires the combination of: (i) realistic dynamics, (ii) applicability to far-from-equilibrium conditions, (iii) controllable sticky binding topology, (iv) variable chemical kinetics, and (v) the ability to treat inhomogeneous systems.

In this paper we develop and validate a model, based on those employed in Refs. [14], [46], and [48], which shows all these characteristics. Much of the physics of amorphous polymer melts and gels is independent of chemical detail,[4,49] so properties (i) and (ii) are captured by using a bead-spring model[48] for the underlying (nonassociative) polymer physics. We capture properties (iii)–(v) by employing a hybrid molecular dynamics/Monte Carlo (MD/MC) approach with controlled (specifically, binary) bonding and variable chemical kinetics.[14] The combination of properties (i–v) allows the model to be used to obtain many results unattainable with previous methods. A key advance is that our algorithm is parallelizable. In validating and investigating our model, we separate the effects of thermodynamics, kinetics, and polymer physics on AP network dynamics and mechanics. We show that sticky bonding is mappable to a "mean-field" two-state Arrhenius rate model, but that the kinetic rate constants for SB association and dissociation are affected by the fact that the SMs are embedded in polymers.

One of the key aspects of AP networks, which has rarely been examined (for *networks*) in the theoretical or simulation literature, is that sticky bond relaxation can be either kinetically limited (KL) (i.e., limited by the intrinsic rate of bonding and/or debonding) or diffusion-limited (DL) (i.e., when the kinetics are so fast that sticky bond dissociation and recombination events become correlated because newly broken SM pairs tend to recombine before exploring the network cage). Most experimental systems seem to be KL, and this is the case treated by almost all published analytic theories for reversibly associating networks, including transient network models.[22,25] Theories for KL AP networks[20,21,24,26,27] assume that the sticky bond lifetime τ_{sb} is so long compared to all polymeric relaxation times that it controls all important time scales for network relaxation, and therefore that kinetics only affect key network relaxation times through their effect on τ_{sb} (or, alternately, as suggested by recent experiments,[50,51] the inverse dissociation rate constant k_b^{-1}, defined below). We show that the validity of this assumption is questionable, and that there is a wide parameter space, plausibly accessible in experiments, where it is invalid. Note that published theories[13,52–56] for diffusion-limited reactions in polymeric systems, such as those of O'Shaughnessy *et al.*, either are not immediately applicable or have not yet been applied to reversible networks.

Our simulations explore the crossover between the KL and the DL cases. We confirm a key prediction of Rubinstein and Semenov[24] on the role of bond recombination on AP dynamics, specifically that recombination effectively renormalizes the SB lifetime in systems where the sticky bonds are sufficiently strong. However, we show that recombination couples interestingly to the diffusive-kinetic crossover in a way not previously predicted.

We extensively examine the dynamics in quiescent, equilibrium systems. One of the more interesting results is that slowing chemical kinetics increases dynamical heterogeneity[40] in a manner similar to increasing the thermodynamic strength of the sticky bonds. We also examine nonequilibrium "chemical dynamics" (i.e., in systems where the initial sticky bond population is not equilibrated), and non-

linear mechanical properties. The studies of nonequilibrium systems and mechanical properties presented here are limited in number because this paper is intended primarily to illustrate the broad utility of the model.

The organization of the rest of this paper is as follows. In Sec. II we further motivate, describe and extensively validate our model. We also discuss how it differs from those used in previous simulations of APs. In Sec. III we present various results for the equilibrium and nonequilibrium physics of thermoreversible AP networks, and compare to theoretical predictions. Finally, Sec. IV presents a discussion and conclusions. Appendices A and B include technical details of the analyses.

II. MODELS AND METHODS

Of particular interest for the current study, and motivating our modeling approach, are recent experiments performed by the group of Craig.[3,50,51,57–59] These have attempted to *independently* vary thermodynamics and chemical kinetics by making systematic changes in sticky monomer chemistry (based on metal-ligand interactions). Systems with similar static properties show dramatic differences in time-dependent properties that are directly associated with the different kinetics. This effect is quite challenging to capture experimentally because thermodynamics and kinetics are highly correlated for most AP systems (i.e., stronger binding $\leftrightarrow$ slower kinetics[3]), but relatively easy to impose in simulations.

The advantages of including variable kinetics in the model are rather obvious given the above discussion. The advantage of imposing binary bonding (i.e., a SM is at all times bonded to either 0 or 1 other SM) is also relevance to current experiments. Sticky monomers with binary bonding are considered particularly valuable for making thermoplastic elastomers with enhanced melt processability and controllable network architecture.[35,60,61] Real examples include multiple hydrogen bonding monomers such as ureidopyrimidinone (UPy), which have highly directional associative interactions of a strength such that the sticky bonds they form constitute a "reversible alternative for the covalent bond."[6,8,60–62] In the model used here,[46] sticky bonds differ from covalent bonds only by their reversibility and strength.

A. Hybrid MD/MC simulation protocol

Our model is built on the framework of the Kremer–Grest bead-spring model,[48] which has been extensively validated and is known to capture the key physics of linear homopolymer melts[48,63] as well as permanently crosslinked networks.[64] Each AP chain is linear and contains N beads (monomers). Systems consist of N_{ch} chains, so the total number of monomers is $N_{ch}N$. Periodic boundary conditions are imposed in all three directions, with periods L_i along directions $i=x$, y, and z. Values of N_{ch} for $N=50$ range from 700 to 5600; the lowest values are chosen to satisfy $L_i > 2R_{ee}$ (where R_{ee} is the mean chain end-end distance), preventing self interactions. Remaining leading order finite size effects in networks scale as $(N_{ch}N)^{-1/3}$ (Ref. 65) and should be ~2% for the systems considered here.

All monomers have mass m and interact via the truncated and shifted Lennard-Jones (LJ) potential $U_{LJ}(r) = 4u_0[(a/r)^{12} - (a/r)^6 - (a/r_c)^{12} + (a/r_c)^6]$, where r_c is the cutoff radius and $U_{LJ}(r)=0$ for $r > r_c$. Covalent bonds between adjacent monomers on a chain are modeled using the finitely extensible nonlinear elastic potential $U_{FENE}(r) = -(1/2) \times (kR_0^2)\ln(1 - (r/R_0)^2)$, with the canonical[48] parameter choices $R_0 = 1.5a$ and $k = 30u_0/a^2$. In this study, following the majority of bead-spring studies on permanently crosslinked systems (e.g., Refs. 64 and 66), we employ flexible chains with no angular potential. We express all quantities in units of the LJ bead diameter a, intermonomer energy u_0, and the LJ time $\tau_{LJ} = \sqrt{ma^2/u_0}$.

All systems have monomer density $\rho = 0.85/a^3$. We employ two temperatures in this study: $k_BT = 1.0u_0$ and $k_BT = 0.6u_0$. These ambient conditions both correspond to dense polymer melts far above the glass transition temperature T_g; $T_g \simeq 0.35u_0/k_B$ for $r_c = 1.5a$ and decreases with decreasing r_c.[67,68] This far above T_g, melt physics is known to be dominated by the repulsive part of the intermonomer interactions;[4] for convenience, and following convention,[48] we use purely repulsive LJ interactions with $r_c = 2^{1/6}a$. However, including attractive interactions by increasing r_c is trivial, is important to realistically capture T dependent properties, and will be done in upcoming studies.

All simulations are performed using an enhanced version of the LAMMPS (Ref. 69) MD code. Newton's equations of motion are integrated with MD using the velocity Verlet method[70] and typical timestep $\delta t = 0.01\tau_{LJ}$.[71] A Langevin thermostat[72] is used to maintain the temperature. The damping time $\tau_{Lang} = 10 - 100\tau_{LJ}$ is larger than the value typically used ($\tau_{Lang} \simeq \tau_{LJ}$) in bead-spring studies; this reduces undesirable thermostat-driven effects such as alteration of stress relaxation by suppression of hydrodynamic momentum transfer.[73] In this study we employ two "chain lengths." Most studies are performed at $N=50$, which is at or below best estimates of the entanglement length $50 \lesssim N_e \lesssim 85$,[74,75] so the melts can be fully equilibrated by allowing chains to diffuse several R_{ee}.[76] $N=50$ is also a convenient choice of chain length because it has been considered in many previous studies. To elucidate the effects of underlying polymeric structure on AP physics, we also consider monomeric melts ($N=1$) that reversibly sticky bond into dimers.

After the melts are equilibrated, we choose a fraction c_{st} of the monomers to be sticky. For the $N=1$ systems these are chosen randomly. For $N=50$ systems, SMs are placed uniformly along chains: at both chain ends and also at internal monomers $iN/(Nc_{st}-1)$, where $i=1,2,\ldots,Nc_{st}-2$. In this study we use $c_{st}=0.08$ (which is comparable to typical experimental values, e.g, Refs. 35 and 77) so for $N=50$ the SMs are the 1st, 17th, 34th, and 50th monomers in each chain. However, any SM placement can be used, and studies of the effects of altering SM placement at fixed c_{st} are underway; the effects of chemical disorder are known to be significant for stress relaxation.[29,35]

Sticky monomers are identical to regular monomers, except that they form reversible sticky bonds. Figure 1 illustrates the potential energy between sticky monomers as a function of their separation r. SMs (like all monomers) al-
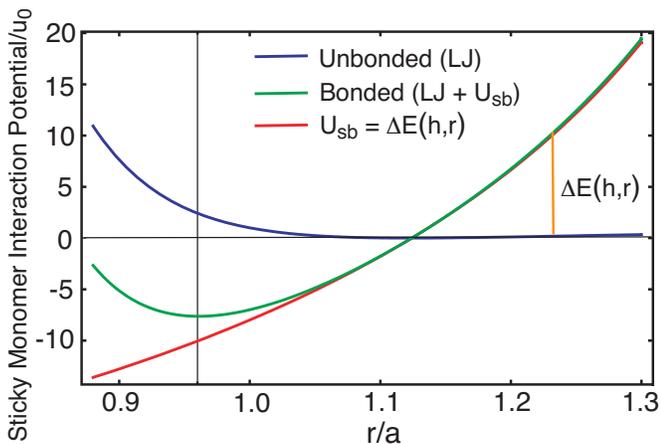
FIG. 1. Sticky monomer interaction potential. Same as in Refs. 14 and 46. Differences in SB formation/breaking rules are noted in the text.

ways interact via LJ interactions, whether bonded or not. Bonded SMs additionally interact via the potential $U_{sb}(r,h)$:

$$U_{sb}(r,h) = U_{FENE}(r) - U_{FENE}(r_0) - h, \quad (1)$$

which is based on the standard covalent FENE potential. Here r_0 represents the equilibrium FENE bond length; $r_0 \simeq 0.96a$, i.e., the minimum of the potential $U_{LJ}(r) + U_{FENE}(r)$. The only difference between the sticky and covalent bond potentials is thus an r-independent, tunable off-set. The same bonding potential was used in Huang *et al.*'s[14,78] studies of equilibrium polymers and a very similar potential was used in Baljon *et al.*'s[46,79] studies of telechelic associating networks. However, our method has several important differences from those of Refs. 14, 46, and 78 (see Sec. II B), so we explain it in detail below.

The potential $U_{sb}(r)$ has several other important features. h represents the sticky binding energy; for $h=0$ a sticky bond can be formed between two monomers separated by r_0 with no change in energy. The associated force $F_{sb}(r)=-\partial U_{sb}/\partial r$, however, is independent of h. Adjusting h is thus a nearly pure way of adjusting the thermodynamics of the sticky bonds without directly altering their chemical kinetics, i.e., the rates of formation and dissociation of sticky bonds.

Formation and breaking of sticky bonds is performed using Metropolis MC.[70] The change in energy required to form a sticky bond between an unbonded pair of SMs is just $\Delta E(r,h)=U_{sb}(r,h)$, and the energy change to break a sticky bond is $\Delta E(r,h)=-U_{sb}(r,h)$. These are the only MC "moves" used, and the acceptance probability of the moves is set by $\Delta E(r,h)/k_BT$.[70] The MC moves are strictly "topological." All spatial motion of bonded SMs is governed by the sticky bond force $F_{sb}(r)$, along with the other forces from LJ and covalent FENE interactions, which are all integrated using MD. One potential difficulty is that only bonded SMs "feel" the force $F_{sb}(r)$, so formation/breaking of SMs creates temporal force discontinuities. However, as will be shown below, this does not seem to cause any spurious behavior.

The system sizes and time scales studied here require simulation on parallel computers; 8 to 64 processors are used in a typical simulation. While MD parallelizes very well,[69] MC is very difficult to parallelize.[80] We therefore perform hybrid parallel MD/serial MC simulations. MC moves are performed once every τ_0 in LJ time units; τ_0 is the MC "timestep." The MD simulation is paused while the parallel-distributed lists of sticky bonds and SM coordinates are gathered onto one processor. For efficiency, Verlet-style pair neighbor lists of SMs are used and of open SM pairs, only those within $r<R_0$ are considered for SB formation. After the SB list is updated, it is distributed back to all processors and the MD simulation resumes. Great care was taken to optimize the MC algorithm to minimize "dead" time on the other processors, but reasonable parallel performance requires $\tau_0 \gg \delta t$. In this paper, except where otherwise noted, we use $\tau_0 = \tau_{LJ}$; see also Sec. II D.

As mentioned above, current experimental trends favor binary bonding sticky monomers, We impose binary bonding through a simple restriction on the MC routine; sticky bond formation is attempted only for pairs of unbonded SMs. The 1-1 bonding restriction imposed here was also assumed in Ref. 24, which eases comparison of our results to theoretical predictions.

Two further technical details of the MC algorithm are noteworthy: (1) we do not allow any SM pair to both break and form a SB (i.e., to break and recombine) during the same MC step. This is a technical violation of detailed balance, but satisfies the weaker "balance" condition sufficient[81] for accurate MC simulation. (2) we do not allow "bond switching" moves within a single MC step. That is, for SMs V, W, X, Y, we do not allow moves of the form

$$V - W + X \rightarrow V - X + W,$$
$$ \quad (2)$$
$$V - W + X - Y \rightarrow V - Y + X - W,$$

or any other more complicated moves. In addition to being difficult to implement in simulations, such processes are unlikely to occur instantaneously in real systems, in part because of steric constraints. Different but analogous rules, suitably modified to the use of SMs with two binding sites each, were imposed in Refs. 14 and 78. SB recombination is a critical aspect of supramolecular polymer physics[24] and is further discussed in Sec. III.

In our model, varying the relative rates of sticky bond formation and dissociation is accomplished by varying h. However, the absolute values of the rates depend on a yet unspecified *kinetic* time scale τ_{kin}. This time can be controlled through the MC routine. At each MC timestep (i.e., every τ_0), a fraction f_{MC} of unbonded SM pairs (of those within range $r<R_0$) and an equal fraction f_{MC} of bonded SM pairs are randomly selected to be considered, respectively, for sticky bond formation and breaking. We have verified this scheme maintains balance[81] for pairs and triplets of SMs for $0.01 \le f_{MC} \le 1$. Thus the average time over which each unbonded or bonded SM pair is considered once for (respectively) SB formation or breaking is $\tau_{MC}=f_{MC}^{-1}\tau_0$, and the parameter τ_{MC} effectively controls the chemical kinetics of the SBs. For a discussion of why we control the kinetics by varying f_{MC} rather than τ_0, see Sec. II D. Small τ_{MC} correspond to fast chemical kinetics,[82] while large τ_{MC} correspond to slow chemical kinetics.

In Sec. III E we perform mechanical tests on various systems. Two types of tests are performed; constant volume deformation and tensile creep. In the constant volume deformation tests, L_z is increased at a true strain rate $\dot{\epsilon} = \dot{L}_z/L_z$, and L_x and L_y are adjusted to maintain constant volume. In the creep tests, a constant (small) stress difference σ_{creep} (relative to the equilibrium hydrostatic pressure in the quiescent state, which is positive for repulsive LJ interactions) is applied along the z direction using a Nose Hoover barostat.[70] This smaller $|\sigma_z|$ produces tensile creep. Both types of tests use $\tau_0 = 0.2\tau_{\text{LJ}}$ to minimize systematic errors.

B. Comparison to previous simulation protocols

It is worthwhile to discuss the simulation method and ambient conditions described above in the context of previous AP simulation studies. The use of a hybrid MD/MC method is a powerful advantage. Pure MC simulations have been performed with lattice[37,38,40,83,84] and off-lattice[36,44] models. These are very effective at studying static properties such as percolative gelation and (in the case of solutions) phase separation, but have limited ability to capture the complex, collective dynamics which occur in bulk polymers, and thus lack properties (i) and (ii). For example, MC cannot, even in principle,[39] capture hydrodynamic effects, which are expected to play an important role whenever momentum transfer is important (e. g. in relaxation of highly stressed systems).

Pure MD studies[41–43,45,47,85] have been used to study static and dynamic properties. While it is better able to capture dynamics and nonequilibrium phenomena than MC, MD studies can not naturally implement controllable sticky bonding topology. Also, MD studies cannot easily impose any control of chemical kinetics without resorting to costly, chemically realistic models. For example, Padding and Boek[86] studied systems intermediate between ours and those studied by Huang et al.;[14,78] a fraction $c_{st} < 1$ of their monomers were allowed to form linear equilibrium polymers, but the FENE-C sticky bonding potential[87] used did not allow for variable kinetics. Thus, in practice, typical MD studies lack properties (iii) and (iv).

The previous works most closely related to the present method are Refs. 14, 46, and 78, who also used hybrid MC/MD with the same $U_{sb}(r)$ [Eq. (1)]. Huang et al.[14,78] also used variable kinetics, but studied equilibrium linear polymers with $c_{st} = 1$ rather than network-forming APs with $c_{st} \ll 1$. Details of the Huang et al.[14,78] method are discussed extensively in Ref. 14. The key differences of our method from Ref. 46 are the imposition of binary bonding and the use of variable τ_{MC} (they used only one $\tau_{\text{MC}} = 0.2\tau_{\text{LJ}}$). Another difference was that Refs. 14, 46, and 78 all used a much stronger thermostat, giving overdamped (Brownian) dynamics.

Many previous studies have used nonspecific (e.g., strengthened attractive LJ or Coulombic) interactions which allow SMs to form arbitrarily many simultaneous SBs.[37,40–43,45,47,83,85] This results in formation of interesting structures such as micelles and micelle-bridge networks, which occur in real AP systems such as associating ionomers

(see, e.g., Ref. 88). However, the (experimental) APs we wish to model tend to form networks more like classical rubbers.

Most previous studies[36,38,40,44,46,85] varied temperature T at fixed SM bonding strength. This does not isolate the effects of T on associative bonding from its other effects such as the dynamical slowdown which occurs in normal (nonassociative) polymers. To get a full picture of AP physics, one should vary both h and T independently.[14] We follow this approach.

Other differences from previous simulation studies are more associated with the systems employed than the methods applied. Many studies have considered only telechelic chains.[41–47,85] Telechelics are appealing in their simplicity, but their network-forming abilities are naturally limited; for binary bonding, at least 3 SMs/chain are required to form good networks. Weakly entangled chains ($N \sim N_e$) may be ideal[8] for technological goals such as enhanced melt processability at high T and network strength at low T. The majority of previous studies have employed extremely short $N \ll N_e$ chains,[38,41–43,46,85] but we consider systems with $N \sim N_e$. Finally, the majority of previous studies have focused on small ρ corresponding to solutions.[14,37,40,42,46,78,83,85] AP solutions exhibit a wide range of intriguing phenomena, in particular competition between gelation and phase separation,[36,38] which, however, we do not wish to consider here. In addition, the presence of solvent can dramatically weaken the effective strength of sticky bonds in real systems;[8,62,77] this effect is beyond the scope of our model. We therefore focus on systems with ρ corresponding to a dense pure melt with no solvent.

Mappings of the bead-spring model to real, dense polymer melts[48] produce different τ_{LJ} in the range of $10^{-10.5 \pm 1.5}s$. Present-day computers can achieve runs (for the system sizes used here) of up to $\sim 10^7\tau_{\text{LJ}} \sim 10^{-3.5 \pm 1.5}s$, but runs this long can not be performed over a broad parameter space. In contrast, sticky bond lifetimes in experimental systems are typically at least $10^{-4}s$, and often many orders of magnitude longer.[50,60,62] Thus any attempt to capture specific SM chemistries and at the same time use systems large enough to study bulk dynamics and mechanical properties would exceed the capabilities of present day supercomputers.[89] Coarse-grained modeling with the goal of studying the dynamics of AP systems *by analogy* is the only currently feasible approach for bulk systems, so we make no attempt to mimic specific chemistries. The only published simulations of which we are aware that model AP networks with specific chemistries[84,90] are pure MC studies that used a very coarse-grained (lattice) bond-fluctuation model[91] and focused on static properties.

C. Static properties: Validation of hybrid MD/MC method

As discussed above, systems contain a total of $N_{st} = N_{\text{ch}}Nc_{st}$ sticky monomers. Due to the binary bonding rules, the maximum number of sticky bonds that can exist in the system at any given time is $N_{st}/2$. If the probability that an SM is bound into an SB is p_{active}, then the total number of
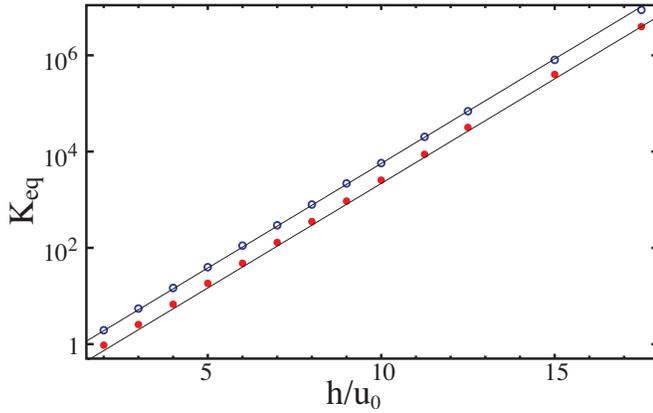
FIG. 2. Sticky association in equilibrium; simulation data and test of Eq. (8). All results are for $N_{ch}N=280\,000$, $c_{st}=0.08$ systems with $k_BT=1.0u_0$ and $\tau_{MC}=1.0\tau_{LJ}$. Closed circles are simulation values of K_{eq} from Eq. (4) for $N=50$ polymers and open circles are for $N=1$ dimer-forming systems. The straight lines are exponential fits, to Eq. (8), for K_{eq}^{TS}.

FIG. 3. Cluster size distribution. $P(M)$ is the probability that a chain will be part of a disconnected cluster of M chains (i.e., the weight fraction of M-clusters). All results are for $N=50$, uniform $c_{st}=0.08$ systems with $k_BT=u_0$ and $h=4u_0$. Data for different kinetic rates are shown: $\tau_{MC}/\tau_{LJ}=1$ (stars), 10 ($\times$), and 100 (+). The apparent preponderance of the lower two rates is an artifact of the plotting procedure. The upward slope at large MW is due to the statistics of small numbers. Results are averaged over 100 statistically independent samples.

SBs in the system is $N_{st}p_{active}/2$. If A represents an unbound SM and A_2 represents a bound SM pair, these factors define the concentrations

$$[A] \equiv \rho c_{st}(1-p_{active}),$$

$$[A_2] \equiv \rho c_{st}p_{active}/2, \tag{3}$$

where square brackets denote concentrations. If the equilibrium value of p_{active} is p^*, then the equilibrium constant for SB association is defined (by the law of mass action for the reaction $A+A \leftrightarrow A_2$) as

$$K_{eq} \equiv \frac{[A_2]}{[A]^2} \equiv \frac{p^*}{2\rho c_{st}(1-p^*)^2} \tag{4}$$

for binary bonding.

Figure 2 shows simulation data in which p^* was evaluated from equilibrated simulations at fixed h and K_{eq} was obtained from Eq. (4). Circles show values of K_{eq} for $N=1$ and $N=50$ systems. As expected, $K_{eq}\sim\exp(h/k_BT)$. The data shown are for $\tau_{MC}=1.0\tau_{LJ}$, but we have verified that p^* is independent of τ_{MC} (to within statistical errors) for all h tested, over the range $\tau_{LJ}\leq\tau_{MC}\leq100\tau_{LJ}$. Because there is an entropy cost $\sim k_BT$ to form a SB, few SBs form for $h<2u_0$. As h/u_0 ranges from 2 to 17.5, the equilibrium constant K_{eq} for $N=50$ varies over more than six orders of magnitude, from 0.96 to 3.9×10^6. This is a wider range of h and K_{eq} than considered in previous simulation studies.[92] A standard finite size scaling analysis of the percolation gel transition is given in Appendix A. For $k_BT=1.0u_0$, percolation occurs at $h=h_{perc}=4.25u_0$, so we consider values of h up to ~4 times above the gelation transition.

Note that the τ_{MC}-independence of p^* allows systems to be equilibrated efficiently using a low τ_{MC}: $\tau_{MC}=\tau_{LJ}$. Higher values of h (for polymeric systems) are impossible to equilibrate on present-day computers with our current method; equilibration is discussed further in Sec. III. However, the highest values of K_{eq} considered here are comparable to those observed in some experiments on multiple-H-bonding SMs.[3,62]

Data from multiple system sizes are also useful in further validating the simulation model. Ben-Naim and Krapivsky[93] have pointed out that systems which reversibly polymerize undergo a nonthermodynamic gelation transition when the fragmentation (in our case, SB breaking) process is too weak. The average number of clusters (aggregates) at any given time is $N_{agg}\equiv N_{ch}/N_n$, where N_n is the number-averaged cluster size (Appendix A). $N_{agg}\equiv N_{ch}$ in the absence of sticky bonding and $N_{agg}\rightarrow1$ in the limit of large h, because all the chains combine into a single network (as in an ideal rubber). Our systems, in the terms of Ref. 93, are "thermodynamic" if and only if: (1) N_{agg} is linearly proportional to N_{ch} below percolation (i.e., for $h<h_{perc}$) and (2) the probability distribution of cluster sizes $P(M)$ (Appendix A) is independent of τ_{MC}. An arbitrary simulation method will not necessarily display a thermodynamic gel transition; failure to do this would be a serious flaw given our goals. We therefore have verified that our model satisfies conditions (1) and (2) for $\tau_{LJ}\leq\tau_{MC}\leq100\tau_{LJ}$, and therefore properly captures reversible gelation. Satisfaction of these conditions appears equivalent to the above-verified condition that p^* is independent of τ_{MC}.[82]

Figure 3 shows data for $P(M)$ at $h=4u_0$ and $k_BT=1.0u_0$ (i.e., just below percolation). The collapse of the data shows[93] that cluster formation/dissociation is an equilibrium processes and supports our arguments that the algorithm satisfies detailed balance for the range of τ_{MC} considered here. Also, $P(M)$ shows some interesting properties which demonstrate that our modeled systems form good (rubberlike) networks. The line shows a fit to a $P\propto(M)^{-5/4}$ power law, which is consistent with the fractal dimension $D_{frac}=4$ of aggregates and the expected power law $\ln(P)\sim-(1+1/D_{frac})\ln(M)$ for networks.[94] In contrast, dense telechelic systems have an exponential $P(M)\sim\exp(-M/\langle M\rangle)$ distribution. The absence of any large exponential contribution in our $P(M)$ at large M indicates that long linear clusters are
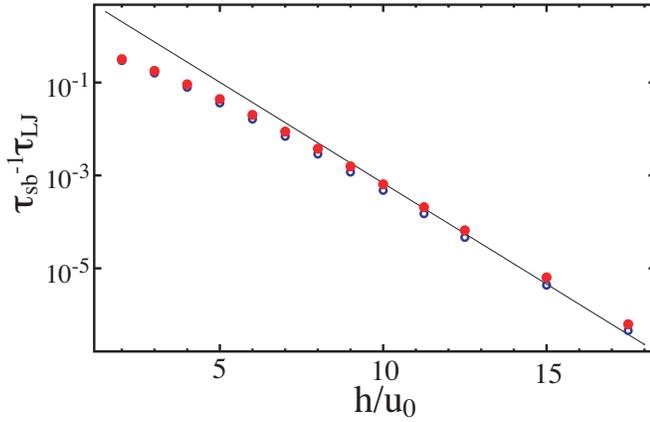
FIG. 4. Sticky bond lifetimes. All results are for 280 000-bead, $c_{st}=0.08$ systems with $\tau_{MC}=1.0\tau_{LJ}$ and $k_BT=u_0$. Closed circles are simulation data for $N=50$ polymers, open circles are data for $N=1$ dimer-forming systems, and the straight line is an exponential "fit," shown only as a guide to the eye.

not common. Therefore, though our parent chains only contain 4 SMs each, we are confident that that is enough to accurately capture AP network physics.

D. SB dynamics and two-state model

Figure 4 shows simulation results for the average sticky bond lifetime, τ_{sb}, in quiescent systems at chemical equilibrium. Simple thermal activation of SB dissociation would suggest exponential behavior, $\tau_{sb}^{-1} \propto \exp(-h/k_BT)$. In fact the results are markedly nonexponential. Interestingly, SB lifetimes in polymeric systems are (apparently) always lower than those in dimer-forming systems. This is consistent with differences in chain connectivity; SBs embedded in polymers experience additional "pulling" forces due to transmission of the random thermal forces (which produce diffusive motion) through covalent bonds along their parent chains. Additional reductions in τ_{sb} could potentially arise from increased steric hindrance to bonding for embedded SMs. While this polymeric effect on τ_{sb} should dependent sensitively on N, c_{st}, and T, to our knowledge it is not included in any theories for AP networks.

The simulation data in Figs. 2 and 4 can be better understood by mapping the MC procedure and $U_{sb}(r,h)$ onto a two-state Arrhenius model for sticky bonding. The model is depicted in Fig. 5. Bonded SM pairs are assumed to have an energy $-h$, unbonded SMs have zero energy, and we introduce an h-dependent barrier $\delta(h)$.

The MC rules described in Sec. II A allow us to assume that sticky bond formation obeys second order kinetics and dissociation obeys first order chemical kinetics, as they should as long as $\rho c_{st} \ll 1/a^3$.[24,95] The SB formation/dissociation process can be represented as the chemical reaction

$$A + A \underset{k_b}{\overset{k_f}{\rightleftarrows}} A_2,\tag{5}$$

where k_f and k_b are the rate constants for SB formation and dissociation. Then the equation for chemical equilibrium is
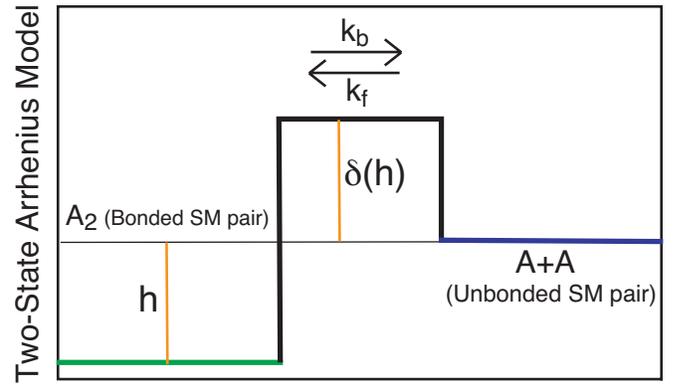
FIG. 5. Arrhenius 2 state model. Refs. 14 and 78 did not introduce an h-dependent δ.

$$k_f[A]^2 = k_b[A_2].\tag{6}$$

In the Arrhenius two-state model the rate constants are given by:

$$k_f = \alpha \exp(-\delta(h)/k_BT),$$

$$k_b = \beta \exp(-(h+\delta(h))/k_BT),\tag{7}$$

where α and β are constants with dimensions of volume $\times$ frequency and frequency, respectively. Note that the above is a mean-field model[12] in that it ignores correlations between sticky monomers (i.e., concentration fluctuations). Thus k_f and k_b (and especially α and β) will in general depend[44] on N, ρ, c_{st}, and (through second order effects such as the variation in ρ at fixed pressure) T.

In thermal equilibrium, Eq. (6) gives the equilibrium constant

$$K_{eq}^{TS} \equiv \frac{k_f}{k_b} = \frac{\alpha}{\beta}\exp(h/k_BT).\tag{8}$$

Equation (8) fits simulation results for K_{eq} very well, as shown in Fig. 2. In AP networks at even higher values of h, Eq. (8) should fail due to "trapped" open SMs (Ref. 44) that cannot find partners, but this effect is negligible for the systems considered here.

We now compare two-state model predictions to simulation data and map the latter to the former. In the two-state model, the mean SB lifetime τ_{sb} is just $\tau_{sb}=k_b^{-1}$. Similarly, the probability that an unbonded pair in the "2A" state (Fig. 5) will jump over the barrier is just $\exp(-\delta(h)/k_BT)$. This is also the success rate $S_{MC} \equiv k_f/\alpha$ for MC SB formation attempts, so $\delta(h)$ can be directly measured from the simulations: $\delta(h)/k_BT = -\ln(S_{MC})$.

In Fig. 6, panel (a) shows simulation results for $\delta(h)$ and panel (b) shows simulation results for $\tau_{sb}^{-1} \exp(\delta(h)/k_BT)$. The latter shows that the perfect exponential decay expected from Eq. (7), $\tau_{sb}^{-1} \exp(\delta(h)/k_BT)=k_b=\beta \exp(-h/k_BT)$, is actually observed. Note that this Arrhenius behavior *was in no way imposed*; it emerges naturally, showing the utility of the two-state model in understanding the behavior of our simulations.

The parameters α and β can be extracted from the data in Figs. 2 and 6. For $\tau_{MC}=\tau_{LJ}$, $\alpha=6.3a^3/\tau_{LJ}$ and $\beta=24/\tau_{LJ}$
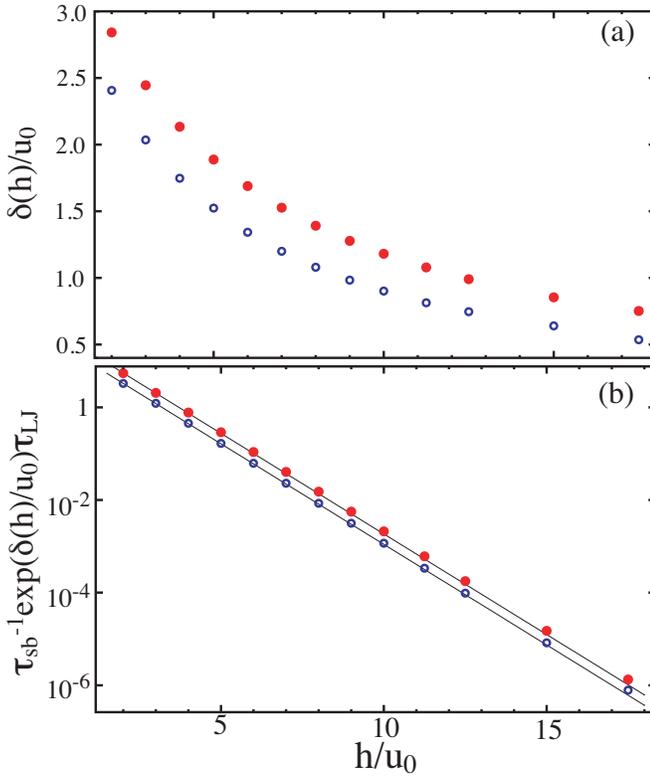
FIG. 6. Validation of method. All results are for 280 000-bead, $c_{st}=0.08$ systems with $\tau_{MC}=1.0\tau_{LJ}$ and $k_B T=u_0$. Closed circles are simulation data for $N=50$ polymers, open circles are data for $N=1$ dimer-forming systems, and straight lines are exponential fits. Data shown are: (a) $\delta(h)/k_B T$, and (b) $\tau_{sb}^{-1}\exp(\delta(h)/k_B T)$.

for dimers, while $\alpha=4.0a^3/\tau_{LJ}$ and $\beta=41/\tau_{LJ}$ for $N=50$ chains. The smaller α measured for polymer-embedded SMs is consistent with the above-hypothesized increased steric constraints. The large rate constant $\beta=41/\tau_{LJ}$ indicates a potential problem with the simulations. β is an effective "attempt frequency" for breaking sticky bonds, which implies that the MC timestep τ_0 should be small compared to β^{-1}. Larger τ_0 will in principle produce systematic errors. The data shown above are for $\tau_0=1.0\tau_{LJ}$, which is large compared to β^{-1}. Simply reducing τ_0 is problematic because it sharply reduces the parallel efficiency of the simulations.

However, we have used values of τ_0 as small as $0.05\tau_{LJ}$, and find that all errors produced by using $\tau_0=1.0\tau_{LJ}$ are small in quiescent systems at equilibrium; for example, the systematic error in τ_{sb} at $h=10u_0$ is about 1%. While the errors in dynamical properties are somewhat larger at small h ($h\ll10u_0$), in this paper we focus on dynamics for $h\geq10u_0$ and use $\tau_0=1.0\tau_{LJ}$. In all cases, all differences produced by smaller τ_0 (at fixed τ_{MC}) are small compared to the differences between systems contrasted in Sec. III, and comparable to our statistical errors, i.e., $\sim$1%. For nonequilibrium systems, however, systematic errors are larger. Thus all nonequilibrium and mechanical-property tests in this paper are performed using $\tau_0\leq0.2\tau_{LJ}$.

In summary, to within our noise, increasing τ_{MC} leaves the static properties of our model AP networks (Fig. 2) unchanged, and changes the sticky bonding dynamics [Figs. 6(a) and 6(b)] only through the prefactor $\tau_{sb}\propto\tau_{MC}^{-1}$. The role

of τ_{MC} in the dynamics therefore appears in the rate constants α and β, which are also proportional to τ_{MC}^{-1}. Increasing τ_{MC} slows down the chemical kinetics of the SBs (both formation and dissociation) relative to the underlying polymeric time scales, while leaving the thermodynamics unchanged.[82] This is why we claim our model can separate thermodynamics and kinetics. The variation in h and τ_{MC} employed here may be thought of as corresponding to "scanning" across chemically different sticky monomers. Given the time scale problem mentioned above, this scanning is only qualitative. However, we show below that it is very useful in understanding AP systems.

III. RESULTS

Previous work has shown[40,46] that the most dramatic changes in dynamics, our primary interest, take place not at h_{perc} but rather at considerably higher h. In this Section we consider systems with $h\gg h_{perc}$ and $p^*\gtrsim0.95$. This is the "physical gel" regime[83] where nearly all chains are (at any moment) part of a single aggregate. A "snapshot" of a physical gel looks much like a crosslinked rubber, yet chains are delocalized and the system can flow at long times. One of the most interesting properties of physical gels is their transition to chemical gels as h increases or T decreases. In this "physical-chemical gel transition" (PCGT), chains become localized[40,46] in a manner analogous to the caging effect produced upon cooling fragile glass-forming systems.[96,97]

For the N, T, and c_{st} considered here, the PCGT occurs[98] at bonding strength $h_{PCGT}>17.5u_0$. The broad range ($5u_0 \lesssim h\lesssim17u_0$) between the percolation (Appendix A) and localization transitions is consistent with the findings of Kumar and Douglas[40] as well as Baljon et al.,[46] who both, however, used constant SB strength and varied T. The broad range is not dependent on having only a few sticky monomers per chain, although increasing Nc_{st} at fixed ρ will broaden the range by lowering h_{perc}. Here we focus on values of h which are well below h_{PCGT}, and thus "in the middle" of the physical gel regime.

Another of the key features of physical AP gels is sticky bond recombination. The concentration $\rho c_{st}(1-p^*)$ of free SMs is small. Moreover, the motion of free SMs is constrained by the neighboring SMs on the same parent chains, which are (transiently but usually) bonded. Thus SM pairs tend to recombine after SB dissociation events. This leads to a second characteristic timescale for individual sticky bonds; in addition to the "bare" lifetime τ_{sb}, there is[24] a larger, "effective" SB lifetime τ^*, which can be thought of as the average time for initially bonded SMs to separate (i.e., no longer recombine) as opposed to merely debond. It is of interest because rheological experiments typically measure τ^*; τ_{sb} is more difficult to access.[3,12,35] Values for τ_{sb} and τ^* (defined more specifically in Appendix B and discussed further in Sec. III B) for a wide variety of systems are given in Table I. We have already shown how τ_{sb} is affected by polymer physics—indirectly through covalent backbone bonds. Now we study the ways in which SB recombination influences and is influenced by the interplay of SB thermodynamics, SB kinetics, and polymer physics. We perform our study

in terms of measurements of diffusion, τ^*, dynamical heterogeneity, nonequilibrium chemical dynamics, and nonlinear mechanical properties. All results presented below are for systems that were first equilibrated for many τ^*. As will be shown, these are best understood by determining whether SB recombination is diffusion-limited or KL.

A. Diffusion

The effect of varying different thermodynamic and kinetic parameters on monomer diffusion [mean squared displacement $\langle(\delta\vec{r})^2(t)\rangle$] is shown in Fig. 7. Panel (a) shows the variation as h is increased at $\tau_{MC}=1.0\tau_{LJ}$ and $k_BT=1.0u_0$. At short times ($t \ll \tau_{sb}$), results for different values of h collapse, showing (as expected) that sticky bonding has little effect on diffusion on these time scales. At larger times ($t \gtrsim \tau_{sb}$) results show a progressive localization and caging effect, similar to that described in Refs. 40 and 46, as sticky bond strength increases. At $h=10u_0$, little localization occurs because[24] τ_{sb} is less than the Rouse time of the chains in the absence of sticky bonding ($\tau_R \simeq 2.6\cdot10^3\tau_{LJ}$). As τ_{sb} increases with increasing h, the curves develop a "shoulder" which illustrate the temporary caging associated with physical gels. This temporary cage becomes permanent as $\tau_{sb}\rightarrow\infty$ (as in a classical crosslinked rubber). Data in panel (a) support our earlier statement that this occurs for some $h \gtrsim 17u_0$.

Panels (b)–(c) show a pair of interesting effects. First, for $h=11.25u_0$ and $k_BT=1.0u_0$, increasing τ_{MC} has the same qualitative effect as increasing h at fixed τ_{MC}. Data for $\langle(\delta\vec{r})^2(t)\rangle$ collapse for t less than the smallest τ_{sb} (i.e., τ_{sb} for the lowest τ_{MC}). For longer times, the data develops a shoulder which increases in width as τ_{MC} increases. Data for an equilibrated system with MC deactivated (i.e., $\tau_{MC}=\infty$) shows chemical gel (ideal rubber) behavior; chains are permanently localized.

Second, data from systems with the same SB thermodynamics (i.e., the ratio $h/k_BT=11.25$) but different ambient conditions ($h=6.75u_0$ and $k_BT=0.6u_0$) shows interesting contrasts which illustrate the interplay of SB dissociation and underlying polymer physics. For $t \lesssim \tau_{sb}$, data for $\langle(\delta\vec{r})^2(t)\rangle$ still collapse, but data from the lower-T systems collapse on a lower value. This is not at all surprising, as polymeric diffusion is well known to slow with decreasing T. However, though h/k_BT is the same, values of τ_{sb} and τ^* are smaller for the lower-T systems, perhaps because h is smaller and SB breaking is favorable at smaller r (see Fig. 1).[99] Thus the diffusion data actually cross over at intermediate time scales (panel c) and the lower T systems show greater mobility at fixed h/k_BT, a most unusual state of affairs. While the case presented here is somewhat artificial because in a real polymer melt ρ would decrease with T and lead to further diffusive slowdown, we believe the point that varying T at fixed SB thermodynamics should change relaxation at different timescales differently should be generally valid. For example, the frequency (ω) dependence of the dynamical moduli $G(\omega;T)$ (Ref. 100) should change with T in nontrivial ways. In other words, time-temperature superposition should be violated.

It is useful to relate the mean squared displacement to the cage size a_{cage} and "escape parameter" $f(t)$ using the definition

$$\langle(\delta\vec{r})^2(t)\rangle \equiv a_{cage}^2 f(t). \qquad (9)$$

In the $\tau_{sb}\rightarrow\infty$ limit, $a_{cage}^3 \sim (\rho c_{st})^{-1}$ is the volume explored by sticky monomers.[101] The chemical gel time t_{chem} is the time at which $f(t)$ approaches unity in this limit. Data for the $\tau_{MC}=\infty$ system in Fig. 7(b) (with $h=11.25u_0$, $N=50$, and $c_{st}=0.08$) shows that $a_{cage}^2 \simeq 23a^2$ and $t_{chem} \sim 10^{4.5}\tau_{LJ}$. For finite τ_{sb}, one can define t_{cage} as a caging time describing the (de)localization of SMs;[40,46] $f(t)$ then has the general form $f(0)=0$, $f(t)\sim1$ for $t\sim t_{cage}$, and $f(t)>1$ for $t>t_{cage}$.

The monomeric diffusion constant D, as measured by $\lim_{t\rightarrow\infty}\langle(\delta\vec{r})^2(t)\rangle \sim 6Dt$, should vary inversely with some "long" characteristic time τ_{long} of the system, roughly defined as the time for chains to diffuse by their end-end distance. Candidates for τ_{long} include τ_{sb} and τ^*. Ref. 24 predicts $\tau_{long} \propto \tau_{sb}$ for weakly binding physical gels and $\tau_{long} \propto \tau^*$ in the strong-binding (near-chemical) limit. Figure 8 shows results for $D\tau_{sb}$, $D\tau^*$, and $8\times10^4\tau_{LJ}D$ from Table I for $h=11.25u_0$, $k_BT=1.0u_0$ systems, over a wide range of τ_{MC}. D decreases with increasing τ_{MC} slower than both $(\tau^*)^{-1}$ and τ_{sb}^{-1}, but it tracks the former more closely than the latter. Thus results for this value of h are apparently intermediate between the "weak" and "strong" physical gel limits described in Ref. 24.

B. Crossover between diffusion-limited and kinetically limited SB recombination

Table I shows τ^* and τ^*/τ_{sb} for all investigated systems. As expected, increasing h at fixed τ_{MC} increases τ^*/τ_{sb}, because for fixed kinetics recombination is more likely for thermodynamically stronger SBs. There are several possible regimes of possible relations between τ^* and τ_{sb} that can be related to diffusion [specifically, $\langle(\delta\vec{r})^2(t)\rangle$] on intermediate timescales. Systems with $\tau_{sb} \gg \min(t_{cage}, t_{chem})$ will exhibit KL sticky bond recombination; in this regime τ^*/τ_{sb} is predicted to be constant.[24] However, if $\tau_{sb} \ll \tau_{cage}$, recombination will be dominated by "correlated" recombinations of SM pairs that have recently dissociated and have not had time to fully diffuse away from one another. This is DL sticky bond recombination. To our knowledge, the DL regime and especially the crossover between DL and KL have not been previously studied for AP networks.

Figure 9 shows the variation in τ^*/τ_{sb} with chemical kinetics for $h=11.25u_0$ systems at $k_BT=1.0u_0$. Over a range of two orders of magnitude in τ_{MC}, the data are well fit by the equation

$$\frac{\tau^*}{\tau_{sb}} = C + \frac{K}{(\tau_{MC})^x}, \qquad (10)$$

where C is the probability of recombination in the KL limit and K is the contribution from diffusion-limited recombination. The exact form of Eq. (10) is not of great consequence;

TABLE I. Variation in τ_{sb}, τ^*, and D with N, T, h, and τ_{MC}. Times are in units of τ_{LJ}. Statistical errors are roughly $\pm 2\%$ or less. All $N=50$ systems have $N_{ch}=1400$ and data are averaged over multiple statistically independent states. * denotes $\tau_0=0.5\tau_{LJ}$ results. $--$indicates calculation is prohibitive or we have insufficient data. Results for D in $N=1$ systems are not presented because they are negligibly affected by sticky bonding.

System	N	k_BT/u_0	h/k_BT	τ_{MC}	τ_{sb}	τ^*	τ^*/τ_{sb}	$10^5\tau_{LJ}D/a^2$
A	50	1.0	10	1	1.55×10^3	7.05×10^3	4.5	18.3
B	50	1.0	10	10	1.54×10^4	2.63×10^4	1.7	8.44
C	50	1.0	10	100	1.53×10^5	1.78×10^5	1.2	2.17
E*	50	1.0	11.25	0.5	2.40×10^3	2.28×10^4	9.5	9.31
DE*	1	1.0	11.25	0.5*	3.35×10^3	2.23×10^4	6.7	N/A
F	50	1.0	11.25	1	4.82×10^3	2.95×10^4	6.1	6.89
DF	1	1.0	11.25	1	6.69×10^3	2.67×10^4	4.0	N/A
G	50	1.0	11.25	2	9.78×10^3	4.05×10^4	4.1	6.07
DG*	1	1.0	11.25	2	1.34×10^4	3.46×10^4	2.6	N/A
H	50	1.0	11.25	5	2.40×10^4	6.42×10^4	2.7	4.81
DH*	1	1.0	11.25	5	3.36×10^4	5.50×10^4	1.6	N/A
I	50	1.0	11.25	10	4.73×10^4	9.70×10^4	2.1	3.11
DI*	1	1.0	11.25	10	6.42×10^4	8.52×10^4	1.3	N/A
J	50	1.0	11.25	$10^{1.5}$	1.55×10^5	2.32×10^5	1.5	1.95
DJ*	1	1.0	11.25	$10^{1.5}$	2.05×10^5	2.30×10^5	1.1	N/A
K	50	1.0	11.25	100	4.82×10^5	6.28×10^5	1.3	0.94
DK*	1	1.0	11.25	100	6.70×10^5	6.85×10^5	~1.02	N/A
L	50	0.6	11.25	1	1.88×10^3	8.02×10^3	4.3	$--$
M	50	0.6	11.25	10	1.91×10^4	3.15×10^4	1.6	$--$
N	50	0.6	11.25	100	1.93×10^5	2.22×10^5	1.2	$--$
O	50	1.0	12.5	1	1.53×10^4	1.23×10^5	8.0	2.79
P	50	1.0	12.5	10	1.55×10^5	3.58×10^5	2.3	1.20
Q	50	1.0	12.5	100	1.53×10^6	2.07×10^6	1.3	$--$
R	50	1.0	13.75	1	4.90×10^4	5.42×10^5	11	$--$
S	50	1.0	13.75	100	4.62×10^6	7.34×10^6	1.6	$--$
T	50	1.0	15	1	1.56×10^5	2.49×10^6	16	$--$
U	50	1.0	15	100	1.48×10^7	2.53×10^7	1.7	$--$
V	50	1.0	16.25	1	5.0×10^5	1.1×10^7	22	$--$

what matters is the broad crossover between regimes and the large change in τ^*/τ_{sb} as a function of kinetics. Nevertheless, since $\tau_{sb}=k_b^{-1}$, Eq. (10) can be interestingly rewritten as

$$\tau^* = \frac{C + K\tau_{MC}^{-x}}{k_b}. \qquad (11)$$

The significance of Eq. (11) is its prediction of a nonlinear dependence of $k_b\tau^*$ on the rate constant k_b for dissociation.

C and K are of course not universal constants, but will depend on h, ρ, c_{st}, T, and N. In practice, one would expect $K\tau_{sb}^x \ll C$ when $\tau_{sb} \gg \min(t_{cage}, t_{chem})$. More physically, the condition $K\tau_{sb}^x \ll C$ *defines* the KL regime, where sticky bond reactions become mean-field in the sense of Cates.[12] The data in Fig. 9 show that one can (at least in our model systems) move from the KL to the DL regimes simply by speeding up the chemical kinetics, if one is in the regime where τ_{sb} is comparable to the underlying polymer relaxation times such as t_{chem}.

For our systems, values of C are close to values of τ^*/τ_{sb} in our "kinetically slow" ($\tau_{MC}=100\tau_{LJ}$) systems, cf. Table I. C increases with h (qualitatively) as predicted by Rubinstein and Semenov.[24] However, while our kinetically slow systems all have $C<2$, the "strong physical gel" theory in Ref. 24 assumes $C\gg1$, so we defer a detailed comparison to that theory to later work. Here we merely make the positive observation that the basic prediction[24] of effective SB lifetime

renormalization $(\tau_{sb}\to\tau^*)$ works well at these relatively small C and (somewhat surprisingly) over the entire studied KL$\to$DL crossover regime. The renormalization $\tau_{sb}\to\tau^*$ accurately captures effective SB dissociation over a very broad parameter space.[102]

On the other hand, an observation apparent from Fig. 9 is that SB recombination is in general only partly polymeric in nature. In the limit of fast kinetics, values for τ^*/τ_{sb} in $N=1$ systems are nearly as high as for $N=50$ systems. However, the lack of a network prevents any caging effects, and so τ^*/τ_{sb} decreases much faster with increasing τ_{MC}, approaching unity (regardless of the value of h) at $\tau_{MC}=100\tau_{LJ}$. This illustrates that the crossover from DL to KL is analogous to a crossover between "dimeric" and polymeric recombination; in other words, chain connectivity (i.e., covalent bonding) becomes increasingly important as kinetics are slowed. While the dimeric contribution to SB recombination cannot be simply subtracted out due to the different $\delta(h)$, these dimeric-versus-polymeric effects on SB recombination have been neglected by previous theories.[103]

C. Recombination and dynamical heterogeneity

Figure 10(a) shows simulation results for the SB recombination probability $P_{recomb}(t)$ (defined in Appendix B) for $h=11.25u_0$ systems with different chemical kinetics. Although there is a small peak in P_{recomb} [not displayed and
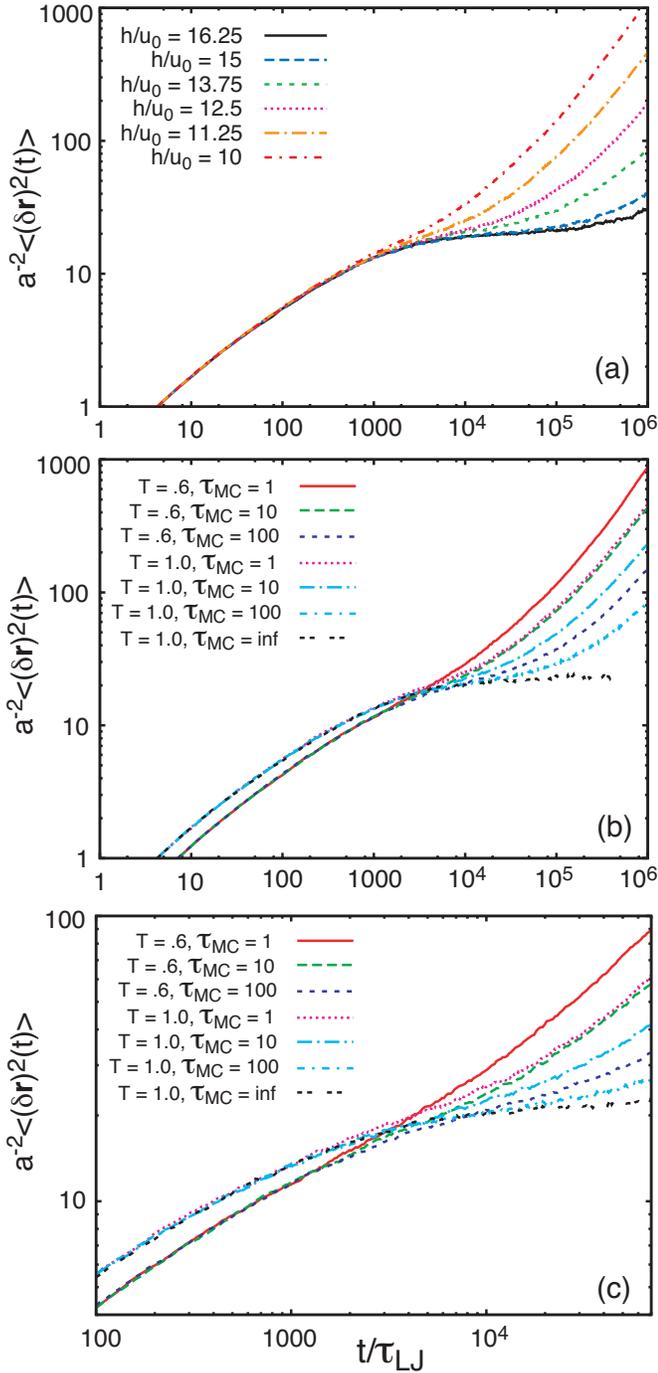
FIG. 7. Diffusion as function of h, T, and τ_{MC}. All systems have N_{ch} =1400 and N=50. Panel (a): $k_B T = u_0$, increasing h. Panel (b): $h/k_B T$ =11.25; $k_B T = u_0$ and $k_B T = 0.6 u_0$, increasing τ_{MC}. Panel (c) is a blowup of (b) showing the crossover. Lines from top to bottom for each T in panels (b)–(c) are for τ_{MC}/τ_{LJ}=1, 10, 100, and (for $k_B T = 1.0 u_0$) ∞. The legends for panels (b)–(c) give T in units of u_0/k_B and τ_{MC} in units of τ_{LJ}.

low compared to the peaks shown in Fig. 10(a)] at very small times $t \sim \tau_{MC}$, the $t^{-5/4}$ behavior predicted[13] for the extreme diffusion-limited case is not found. This indicates none of our systems have "too-fast" kinetics.[14] For $t \gg \tau_0$, our results have the interesting form $P_{recomb}(t) \simeq \exp(-t/\tau^*) - \exp(-t/\tau_{sb})$; a comparison to actual data for τ_{MC} =$10\tau_{LJ}$ is shown.

This form of $P_{recomb}(t)$ has a maximum at the "delocalization" time
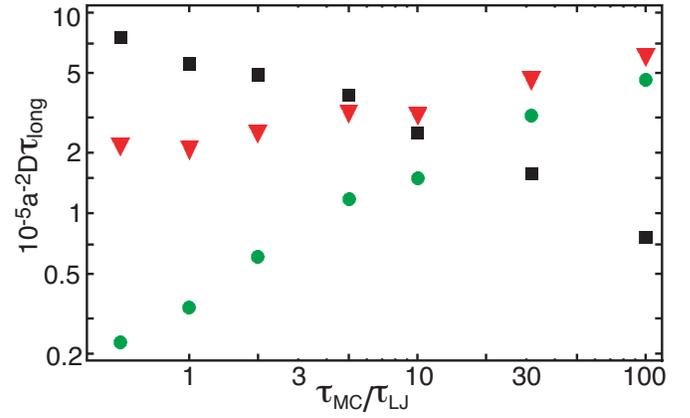
FIG. 8. Scaling of diffusion with various candidate "long" relaxation times. Data shows $D\tau_{long}$ for $\tau_{long}=\tau_{sb}$ (circles), $\tau_{long}=\tau^*$ (triangles), and $\tau_{long}=8 \times 10^4 \tau_{LJ}$ (squares). The last value is chosen so the "bare" diffusion constant D can be shown on the same plot. All results are for systems with N_{ch} =1400, N=50, $h=11.25u_0$ and $k_B T=1.0u_0$. $D\tau_{MC}$ is not shown because $\tau_{sb} \propto \tau_{MC}$.

$$\tau_{deloc} = \tau_{sb} \frac{y \log y}{y-1}, \tag{12}$$

where $y = \tau^*/\tau_{sb}$. Bonded SM pairs trend towards moving away from each other after τ_{deloc}. Furthermore,

$$\frac{\tau_{deloc}}{\tau^*} = \frac{\log y}{y-1}, \tag{13}$$

which becomes small for $y \gg 1$. This suggests τ_{deloc} (in addition to τ^*) might be a key relaxation time in systems with large y. However, this is speculative and needs further verification.

A useful measure of relaxation in complex fluids is the "non-Gaussian" parameter

$$\Lambda(t) = \frac{3\langle \delta r^4(t) \rangle}{5\langle \delta r^2(t) \rangle^2} - 1, \tag{14}$$

which is zero for normal diffusion and positive for systems where some particles move anomalously fast,[42] particularly for "hopping" type motion. Λ has been shown to be relevant to the structural relaxation of supercooled liquids and dynamical heterogeneity.[96] The time t_{deloc} at which Λ is maximized and the maximum value $\Lambda_{max} = \Lambda(t_{deloc})$ both increase with decreasing T in various systems, including APs,[40,42,46] as localization increases. t_{deloc} may be regarded as a crossover time after which the system begins to show liquidlike behavior.

Figure 10(b) shows the effect of kinetics on $\Lambda(t)$. The effect of slowing kinetics at fixed $h/k_B T$ is similar to the effect of increasing $h/k_B T$ observed in previous studies.[40,46] It is interesting that increasing τ_{MC} increases dynamical heterogeneity. The probable reason is that increasing τ_{MC}, even though it leaves p^* unaffected, decreases the likelihood of multiple closed SBs on the same chain breaking within a short time period. This is consistent with the idea[21] that coherent breaking of nearby SBs along a chain eases large-scale motion. The increasing dynamical heterogeneity with increasing t_{cage} is consistent with other results showing Λ_{max}
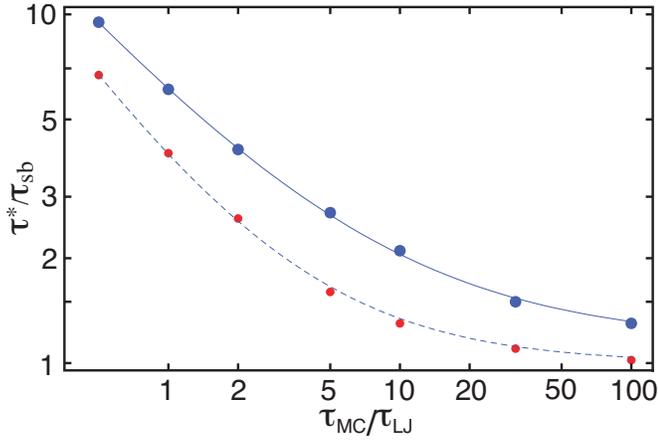
FIG. 9. Crossover from DL to KL sticky bond recombination for $h = 11.25u_0$ and $k_BT = 1.0u_0$. All systems have 70 000 beads, with $c_{st} = .08$. The upper data set is for $N = 50$ polymers and the lower is for $N = 1$ dimer-forming systems. The fastest-kinetic systems ($\tau_{MC} = 0.5\tau_{LJ}$) use $\tau_0 = 0.5\tau_{LJ}$, and all others use $\tau_0 = \tau_{LJ}$. The solid line shows a fit to Eq. (10) with $C = 1.15$, $K = 4.98\tau_{LJ}^x$ and $x = 0.74$. The dashed line shows a fit with C set to 1, $K = 2.97\tau_{LJ}^x$ and $x = .94$.

increases as localization "transitions" are approached, e.g., stretched-exponential relaxation of finite clusters.[41]

The data in Figs. 9 and 10 also clearly show that $t_{deloc} \simeq \tau_{deloc}$ in systems where recombination is likely (i.e., when τ^*/τ_{sb} is large compared to 1), and thus that delocalization is closely related to individual sticky bonds finding new partners in a hopping type motion. However, these delocalization times are large compared to t_{cage}. This is not surprising, as full delocalization should occur only when chains have lost all memory of their initial SB topology; this "memory" time is inherently polymeric in that it must increase with increasing Nc_{st}, similarly to a Rouse or reptation time.[4] Interestingly, the peaks of Λ are broader than those of P_{recomb}. This also likely arises either from cluster effects[24,41] or other underlying many-SM phenomena that ultimately arise from the polymer physics, i.e., the covalent connectivity of the parent chains.

D. Nonequilibrium chemical dynamics

An important feature of our model is its ability to accurately capture the dynamics of systems in which the sticky bonds are not in thermal equilibrium. The evolution of SB concentration is, following Eq. (5), given by

$$[\dot{A}_2] = k_f[A]^2 - k_b[A_2], \tag{15}$$

which after plugging into Eq. (3) and simplifying becomes

$$\dot{p}_{active} = 2k_f\rho c_{st}(1 - p_{active})^2 - k_b p_{active}. \tag{16}$$

Equation (16) has an analytic solution. For the special initial condition $p_{active}(t) = 0$ at $t = 0$, the solution is

$$p_{active}(t) = d - \frac{(d^2 - 1)\tanh(2z\sqrt{d^2 - 1}\,t) + d\sqrt{d^2 - 1}}{d\tanh(2z\sqrt{d^2 - 1}\,t) + \sqrt{d^2 - 1}}, \tag{17}$$

where $z = \rho c_{st} k_f$ and $d = 1 + k_b/4z$.

Figure 11 compares this analytic prediction to simulation
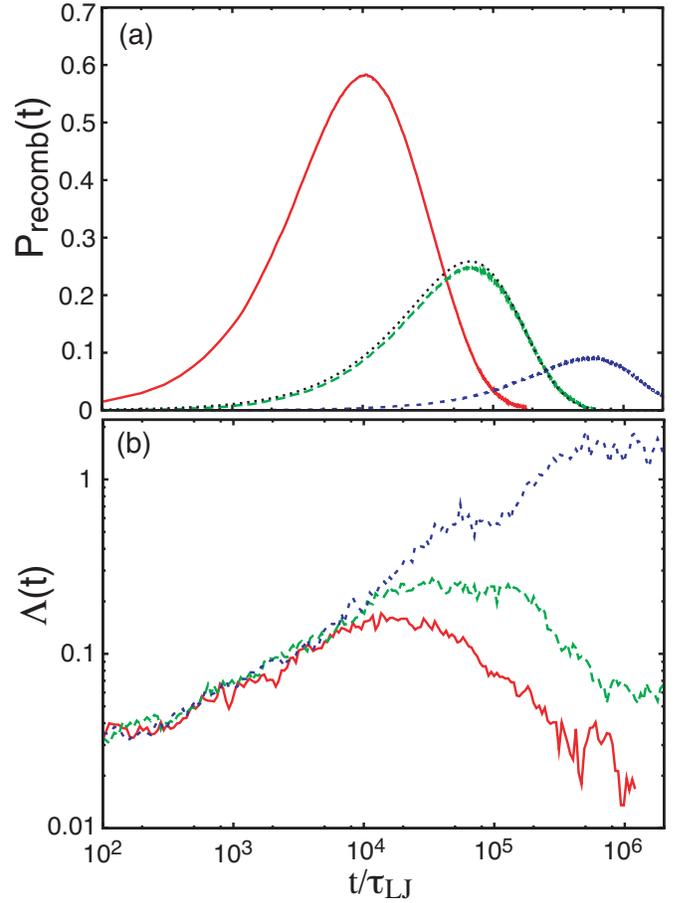
FIG. 10. SB recombination and dynamical heterogeneity. All systems have $N_{ch} = 1400$, $N = 50$, $h = 11.25u_0$ and $k_BT = 1.0u_0$. Lines from top to bottom are for $\tau_{MC}/\tau_{LJ} = 1$, 10, and 100. Panel (a): $P_{recomb}(t)$. The black dotted line is $\exp(-t/\tau^*) - \exp(-t/\tau_{sb})$ for $\tau_{MC} = 10\tau_{LJ}$. Panel (b): $\Lambda(t)$.

results for $p_{active}(t)$ upon activation of sticky bonding for two systems with the same value of h/k_BT but different values of h and k_BT. Values of z and d in Eq. (17) are taken from fit values of α, β, and the measured value of $\delta(h)$ as reported in Sec. II; note that these vary somewhat with T, giving different p^* at the same h/k_BT. Data agree excellently with predictions at short and long times. The merely qualitative agreement at intermediate times is no cause for concern, but is an interesting "feature," because Eq. (16) ignores all physics arising from the important fact that the sticky monomers are embedded, at a concentration c_{st}, in chains of length N, in a dense polymer melt. The slower convergence of simulation results for $p_{active}(t)$ relative to the prediction of Eq. (17) is consistent with such polymeric effects; better agreement is observed for dimer systems. As expected, the polymeric slowdown is greater at lower T.

The results above demonstrate the ability of our method to capture the effect of polymer physics on nonequilibrium chemical dynamics. Thus, as in Ref. 14, it can be used to perform "T-jump" simulations. These may be useful in analyzing phenomena observed in recent real T-jump experiments; nonequilibrium sticky bond behavior is also expected to play a role in self healing AP systems.[9] Note that, for example, the timescale over which p_{active} changes in Fig. 11 is smaller than the equilibrium τ_{sb} ($1.5 \times 10^3 \tau_{LJ}$ for $h = 10u_0$).
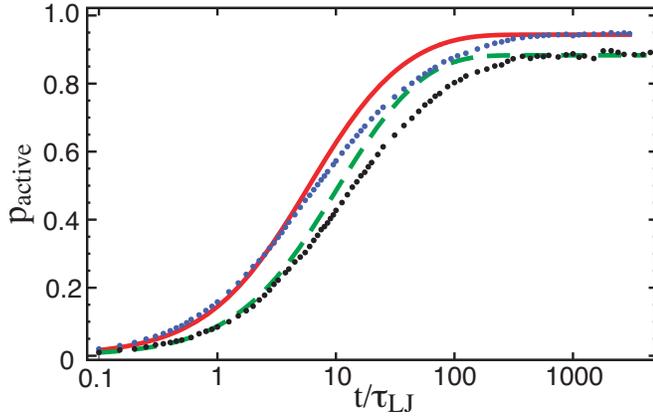
FIG. 11. Nonequilibrium capability of method: h-jump. Solid (dashed) lines are the predictions of Eq. (17) and upper (lower) circles show simulation data for $h=10u_0$, $k_BT=1.0u_0$ ($h=6u_0$, $k_BT=0.6u_0$) for an $N_{ch}=5600$, $N=50$ system after turning on sticky bonds. Simulations used $\tau_0=0.05\tau_{LJ}$.

Similarly, the timescale of self healing at a fractured surface (where p_{active} is out of equilibrium) was found to be smaller than the time scale for near-equilibrium creep relaxation.[9]

E. Nonlinear and nonequilibrium mechanical properties

Figure 12(a) shows results for creep tests of two systems with different thermodynamics and kinetics but the same τ_{sb} ($\tau_{sb}\simeq1.5\times10^4\tau_{LJ}$). Both tests were performed at $k_BT=1.0u_0$. The applied stress difference $|\sigma_z-(\sigma_x+\sigma_y)/2|=0.01u_0/a^3$ is small. At times $t\ll\tau_{sb}$, the extension ratio $\lambda_z=L_z/L_z^0$ is the same for both systems. For $t\gg\tau_{sb}$, λ_z is nearly linear in $\ln(t)$, implying that the flow is nearly linear creep. The system with stronger bonds and greater SB recombination shows greater resistance to flow, i.e., a smaller creep compliance.

It is interesting to relate the creep response to the quiescent dynamics. Figure 12(b) shows (quiescent) diffusion in the same systems. The creep response and diffusion are remarkably similar; the onset of more rapid creep in the $h=10u_0$, $\tau_{MC}=10\tau_{LJ}$ system under stress corresponds directly to the onset of (relative) delocalization in the quiescent state. This is consistent with a recent experiment showing connections between creep behavior and linear rheology in reversible supramolecular networks.[9]

Next we consider constant volume tension simulations at $h=11.25u_0$, $k_BT=u_0$, and various τ_{MC}. These simulations can be considered to be an extension of Ref. 104, which allowed breaking and formation of interchain bonds only at a few (discrete) strains; here SBs break and reform continuously. Here we present results for $\dot\epsilon=10^{-5.5}/\tau_{LJ}$. Simulations at other $\dot\epsilon$ were considered; larger values $\dot\epsilon\gtrsim t_{cage}^{-1}$ make the non-SB-related viscous stress contribution unacceptably large, while smaller values lead to more sticky bond breaking/formation during deformation than is desirable at the values of h and τ_{MC} considered.

Figure 13 shows the stress difference $|\sigma_z-(\sigma_x+\sigma_y)/2|$. With MC deactivated during deformation ($f_{MC}=0$ or equivalently $\tau_{MC}=\infty$), the stress takes a form close to that predicted by entropic elasticity:[105] $\sigma=G_eg(\lambda)$, where $g(\lambda)=\lambda^2-1/\lambda$
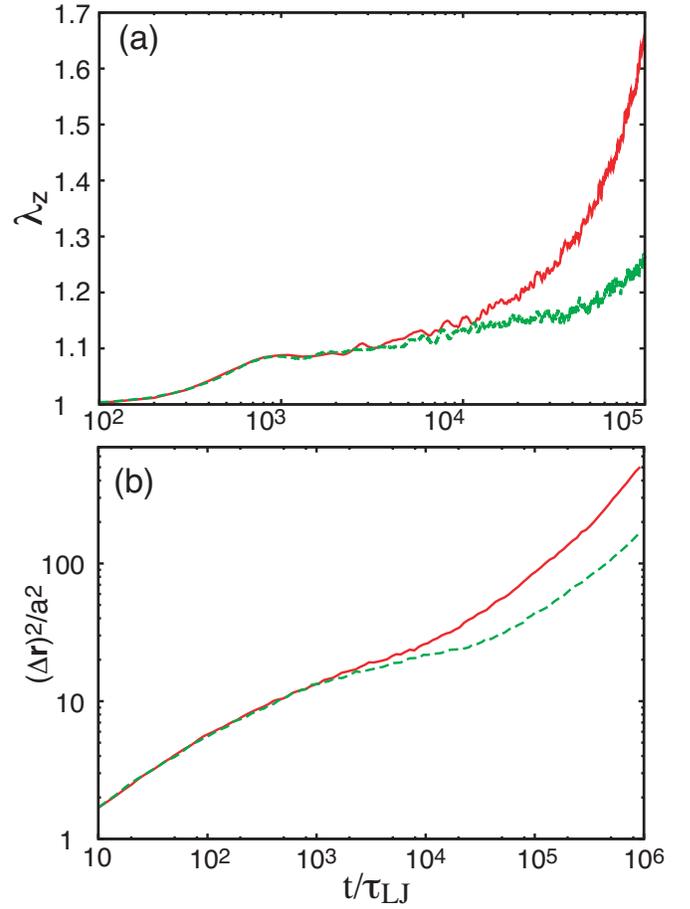
FIG. 12. Linear creep and quiescent diffusion for two systems with the same τ_{sb} but different SB recombination. Results are for systems with $N_{ch}=5600$, $N=50$, and $k_BT=1.0u_0$. Panel (a) stretch $\lambda_z=L_z/L_z^0$ under a creep stress $\Delta\sigma=0.01u_0/a^3$. The upper curve is for $h=10u_0$, $\tau_{MC}=10\tau_{LJ}$ and the lower curve is for $h=12.5u_0$, $\tau_{MC}=1.0\tau_{LJ}$. Panel (b): mean squared displacement for the same systems in the *quiescent* state.

and $\lambda=L_z/L_z^0$ as above. G_e is predicted to be $Nc_{st}p_{inter}k_BT/2$, where $p_{inter}<p^*$ is the interchain portion of active SBs; the actual value from the fit, $G_e=0.028u_0/a^3$, is close to the predicted value $0.031u_0/a^3$, indicating viscous stresses are low at this strain rate. The fit is performed for $g\leq5$; the nonlinear behavior observed at higher g arises from finite extensibility of chain segments between crosslinks (as in standard nonlinear rubber elasticity[105,106]).

The simplest result, assuming that $\dot\epsilon^{-1}\gg\tau_{free}$, $\tau_{sb}\gg\tau_{free}$ (here τ_{free} is the lifetime of unbonded SMs), and that SB breaking and formation rates do not vary with stress/strain, so that stress memory is lost like $\exp(-t/\tau_{sb})$, is[18]

$$\sigma_z(\lambda)=G_e\exp(-\ln(\lambda)/\dot\epsilon\tau_{sb})$$
$$\times\left[g(\lambda)+\frac{1-\lambda^2}{1-2\,\dot\epsilon\tau_{sb}}+\frac{1/\lambda-1}{1+\dot\epsilon\tau_{sb}}\right]\qquad(18)$$

where the first term in brackets is classical rubber elasticity and the second two terms reflect new SBs created during deformation. The $\ln(\lambda)$ comes from the constant true strain rate $\dot\epsilon=\partial\ln(\lambda)/\partial t$.

In Fig. 13, stress-strain results from simulations are compared to predictions from Eq. (18) using values for τ_{sb} from Table I and the value of G_e from the $\tau_{MC}=\infty$ system are
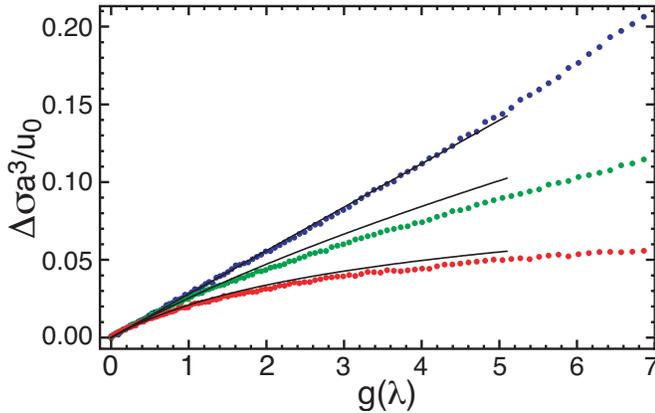
FIG. 13. Constant volume tension simulations for systems with different SB kinetics. The stress difference $\delta\sigma = \sigma_z - (\sigma_x + \sigma_y)/2$ is plotted against $g(\lambda)$ $= \lambda^2 - 1/\lambda$. Systems have $N_{ch} = 5600$, $N = 50$, $h = 11.25u_0$, $k_B T = 1.0u_0$, and the strain rate is $\dot{\epsilon} \equiv \dot{\lambda}/\lambda = 10^{-5.5}/\tau_{LJ}$. These runs use $\tau_0 = 0.2\tau_{LJ}$ for greater accuracy. Data from top to bottom correspond to $\tau_{MC} = \infty$ (no SB breaking/forming allowed during deformation), $\tau_{MC} = 100\tau_{LJ}$ and $\tau_{MC} = 10^{1.5}\tau_{LJ}$. The solid lines are predictions of Eq. (18), with the value of G_e taken from a fit to the $\tau_{MC} = \infty$ data and values of τ_{sb} taken from Table I.

shown. We confine the comparison to the linear regime ($g \leq 5$) to avoid confusion. Sticky bond recombination might be expected to slow relaxation. However, stress relaxation is actually faster than predicted by Eq. (18). We have verified that p_{active} does not decrease during deformation. It appears that instead, τ_{sb} is reduced by stress. A detailed examination of this effect and comparison of nonlinear mechanical properties to theories, e.g., Ref. 28 and transient network models, e.g., Refs. 18, 22, and 25, is deferred to later work, but the data presented above suggests traditional theories will break down in the nonlinear regime.

IV. DISCUSSION AND CONCLUSIONS

We have performed an initial set of simulations using a new coarse-grained model for APs. The MD/MC hybrid algorithm and variable chemical kinetics allow for greater realism and flexibility than in previous simulations of AP networks. Further, the 1-1 sticky monomer binding topology imposed here reflects current experimental trends. The model was extensively validated and is able to accurately model equilibrium dynamical properties, nonlinear mechanical properties, and far-from-equilibrium systems. We studied the model over a very broad parameter space. While have emphasized that we study APs by analogy because simulations of chemically realistic AP networks are not yet computationally feasible,[89] our results should nevertheless aid in "rational"[51] design of AP systems, especially in transition regimes such as those discussed in this paper.

The key results presented here focused on separation, comparison and contrast of thermodynamic and chemical-kinetic effects on SB recombination, the motion of individual chains, and bulk mechanical properties. As expected, instantaneous network structure was independent of kinetics at fixed thermodynamic conditions (i.e., sticky bond strength $h/k_B T$), and relaxation times increases with increasing $h/k_B T$. Similarly, at fixed h and $k_B T$, relaxation slows as the chemical kinetics are slowed. This was illustrated by mea-

surements of monomer diffusion. In the physical gel regime, monomers experience a temporary caging similar to that found in glasses. This caging effect strengthens as SB strength is increased[40,46] but also as kinetics are slowed at fixed SB strength. Analyses showed that chains become increasingly localized in a manner similar to that associated with the increase in dynamical heterogeneity in non-AP melts approaching the glass transition. Of course, the analogy should not be taken too far; in AP networks the caging is produced only by sticky monomers while in systems approaching T_g it is produced by hard core repulsions of all monomers.

We find that, as expected, the chemical kinetics controlling τ_{sb} are mean-field[12] and mappable to a two-state Arrhenius model. However, as kinetic rates are increased and SB recombination becomes nonkinetically limited, the relation between the SB lifetime τ_{sb} and other relaxation times, such as the effective SB lifetime τ^*, becomes decidedly nontrivial. This was explicitly related to the crossover to DL SB recombination. A new quantitative relation between τ^* and τ_{sb} was found. Such relations should be of interest because rheological experiments can typically only access τ^*, which is assumed to control stress relaxation (e.g., because scission followed by quick recombination does not relax stress).[3,12,35]

While the results for T-variation and mechanical properties presented here were limited and somewhat preliminary, we showed examples which illustrate important effects. Analysis of diffusion on intermediate time scales illustrated the point that sticky bond and underlying polymeric timescales will in general vary differently with T, affecting the "interplay" in nontrivial ways. In two systems with the same τ_{sb}, systems with different propensities for SB recombination showed the same creep flow at short times, but those with greater recombination showed a smaller long-time (DC) creep compliance. These differences were directly related to the faster delocalization of chains in the *quiescent* state for systems with less recombination. Constant volume deformation studies showed that, as expected, τ_{sb} is reduced by stress. Extensive studies of the variation with T (in systems including attractive nonbond interactions for greater realism) and more detailed analyses of nonlinear mechanical properties are underway.

Nearly all published analytic theories for AP networks assume a single controlling relaxation time, either τ_{sb} or τ^*, controls the ultimate relaxation properties (i.e., other relaxation times scale with the controlling time). We showed through various measurements that there is a broad parameter space (both in terms of SB strength and kinetics) within the physical gel regime where the "scaling" assumption fails. This parameter space corresponds to the conditions (1) τ^*/τ_{sb} is larger but not "much larger" than unity, and/or (2) SB recombination is not KL. Deviations from this scaling behavior due to multiple controlling relaxation times have been observed,[51,58] but had not yet been well understood. These deviations had been previously assumed to arise from chemical disorder, and this is no doubt partially correct, but as discussed in this paper, they also arise from the interplay between SB thermodynamics, kinetics, and polymer physics. If either (1) or (2) hold, both traditional[22,25] and more

sophisticated[21,24,26] theories should fail to predict the mechanical properties of AP networks. This is not meant as a criticism of the theories, merely an observation that there is a broad parameter space where one or more of their assumptions fail.

The DL and KL limits have been discussed by O'Shaughnessy and Yu;[13] they, respectively, correspond to dominance of the K-term and C-term in our Eq. (10). Conditions under which systems may lie outside the KL limit and/or evidence for systems which lie outside it are also discussed, to some extent, in the context of AP networks in Refs. 43, 44, and 50. Coupling between SB and polymeric relaxation has also been treated approximately by Cates[12] and Leibler et al.,[21] respectively, for linear EP systems and AP networks where recombination is improbable. Among published analytic theories for AP networks, Refs. 21 and 55 qualitatively treat nonkinetically limited systems and Ref. 24 treats SB recombination. Our results are consistent with the argument of Ref. 55 that reaction rates (here defined as nonrecombinative SB exchange) reach the mean-field/KL regime only when reaction is slow compared to the longest "underlying" polymeric relaxation time [in our case $\min(t_{cage}, t_{chem})$].[107] Interestingly, Refs. 52 and 54 suggest that MF kinetics would apply to τ^* as well as τ_{sb} in dimensions $d \geq 4$ because $\langle |\delta \vec{r}|^2 \rangle \sim t^y$ necessarily has $y \leq 4$ (i.e., no diffusion-limited regime is possible). This suggests that diffusion-limited SB recombination, which increases τ^*/τ_{sb}, will increase in importance in AP systems with effectively reduced dimensionality (e.g., very thin films or "pores"). Combining the approaches of Refs. 21, 24, and 55 may be useful for developing optimal analytic theories of these systems, at least for T well above T_g. However, we are not aware of any quantitative discussion of the crossover between the DL and KL regimes such as presented here.[108]

The rheologically simple (i.e., all key relaxation times scale with τ_{sb})[50,51] behavior observed in the majority of experiments on AP networks indicates they exhibit KL behavior. Note that these experiments have shown KL behavior, even though their values of p^* are comparable to values for systems which in our model exhibit DL behavior at low τ_{MC}. This likely arises from the slow kinetics caused by the bulkiness and directional interactions of real sticky monomers. Creating (real) strong-binding SMs with even faster kinetics seems to be difficult. However, one can move out of the KL regime (at fixed kinetic rates) simply by slowing the polymeric relaxation times, e.g., by going to higher concentrations and/or entangled chains. Experiments in this regime are underway,[58] and seem to show a breakdown of the simple scaling; for example, they show an unusually high power law dependence of viscosity on concentration, which appears to arise because τ_{sb} is of order the time scale for reptation. Ref. 51 also shows an apparent (if weak) breakdown in scaling at the highest frequencies considered. In the context of these observations, we note that the parameter space where (1) and or (2) hold may be of greatest interest for designing materials with novel mechanical properties. Our model seems well suited to aid in understanding the complicated behavior of AP networks in this regime.

Here we have left the regime of physically entangled

APs, which is the regime treated by some key analytic AP theories,[21,26,27] untouched. Also, the interplay described in this paper should depend on the details of sticky monomer arrangement along chains, not just N and c_{st}. Studies of systems with a wide range of N and c_{st}, as well as inhomogeneous (chemically disordered) systems, are underway.

In real AP networks the sticky and regular monomers have different sizes and chemistries. Thus an obvious extension of our model would be to increase the differences between the sticky and normal monomers. For example, changing secondary interactions may induce microphase separation.[43,109] Another extension would be use of a more realistic sticky bonding potential such as those used to model H-bonds (see, e.g., Ref. 110 and references therein), but here we have focused on chemistry-independent properties. A coarse-grained way to capture this would be to keep the binary bonding rules, but include more than one sticky site per SM; this would increase the directionality of bonding, which is a key to the performance of the UPy systems.[60] Finally, nanocomposites of APs,[111] where the presence of nanoparticles may or may not[112,113] affect single-chain structure but will certainly affect AP network structure, should have even richer physics than regular polymer nanocomposites.

APPENDIX A: PERCOLATION GEL TRANSITION

Let $N_i^{cl} \equiv N_{ch}P(N_{ch}, i)$ be the average number of disconnected clusters of i chains in a system of N_{ch} chains with periodic boundary conditions (at any given time). $P(N_{ch}, i)$ is a cluster size probability distribution with $\sum_{i=1}^{N_{ch}} i P(N_{ch}, i) \equiv 1$. The number-averaged cluster size is then $N_n = N_{ch}\sum_{i=1}^{N_{ch}} i P(N_{ch}, i)$ and the weight averaged cluster size is $N_w = N_n^{-1} N_{ch}\sum_{i=1}^{N_{ch}} i^2 P(N_{ch}, i)$. For an infinite system, the percolation gel transition occurs (by definition) when p^* exceeds p_{perc}; N_w diverges at $p^* = p_{perc}$.[49] However, computer simulations are limited to finite N_{ch}, and the value of N_w cannot exceed N_{ch}. Thus the N_{ch}-dependent geometric percolation $p^* = p_{span}$ (at which one aggregate spans the system) approaches p_{perc} from below as $N_{ch} \to \infty$.[64] Fortunately, p_{perc} and h_{perc} (the value of h at which $p^* = p_{perc}$ in an infinite system) can be estimated for finite N_{ch} using a standard finite size analysis.[70]

We perform such an analysis, following Ref. 92. Figure 14 shows this analysis for $N = 50$, $c_{st} = 0.08$ systems at $k_B T = 1.0u_0$. The figure plots the rescaled variables $(N_w/N_{ch})^{-\gamma} N_{ch}^{-\gamma/3\nu}$ versus $((p_{perc} - p^*)/p^*)N_{ch}^{1/3\nu}$.[92] $p^{perc} \simeq 0.40$ is close to the predicted value $1/(Nc_{st}p^*f_{inter} - 1)$,[64] where
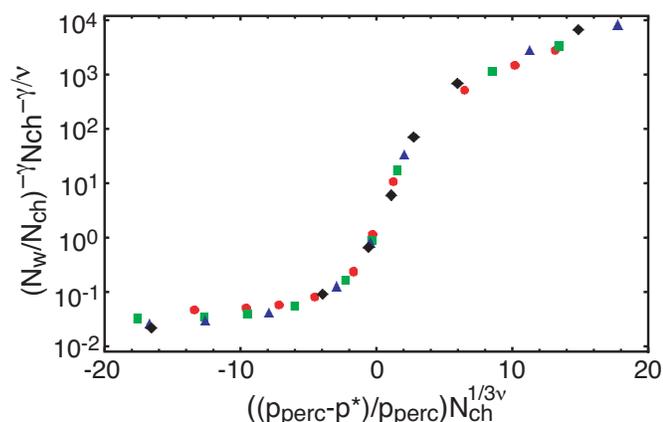
FIG. 14. Finite-size analysis of the percolation gel transition. Data are at $k_BT=1.0u_0$ for $N_{ch}=700$ (circles), $N_{ch}=1400$ (squares), $N_{ch}=2800$ (triangles), and $N_{ch}=5600$ (diamonds) are shown. $p_{perc}\simeq 0.40$.

f_{inter} is the fraction of SBs which are interchain rather than intrachain. The exponents used to collapse the data in the figure are $\gamma\simeq 1.7$ and $\nu\simeq 1.2$; considering a narrower range of h gives values consistent with predictions from the theory of critical phenomena ($\gamma\simeq 1.8$, $\nu\simeq 0.9$).[114] These exponents been extensively discussed in the literature[38,64,92] and need not be discussed further here. In the figure, h increases going from right to left, and percolation occurs at $h_{perc}\simeq 4.25u_0$.

APPENDIX B: NUMERICAL ANALYSIS OF SB RECOMBINATION

In this paper, the sticky bond self-correlation function $P_{auto}(\triangle t)$ is the probability that a bond between two given SMs exists both at times t and $t+\triangle t$, while the SB "transition function" $P_{trans}(\triangle t)$ is the probability that the bond exists *continuously* between times t and $t+\triangle t$. The SB "recombination function" $P_{recomb}(\triangle t)\equiv P_{auto}(\triangle t)-P_{trans}(\triangle t)$ is the probability that a pair of SMs will be bonded at two times separated by $\triangle t$ but that the bond between them has broken at least once during that interval. We find P_{trans} exhibits nearly single-exponential decay, $P_{trans}=\exp(-t/\tau_{sb})$ for all systems, while for $h\gtrsim 10u_0$, P_{auto} also shows exponential decay for (at least) the first decade. Values of τ^* presented here are measured from fits to $P_{trans}=\exp(-t/\tau^*)$. All quantities are averaged over all SM pairs and all t.

[1] M. Rubinstein and A. V. Dobrynin, Curr. Opin. Colloid Interface Sci. **4**, 83 (1999).
[2] L. Brunsveld, B. J. B. Folmer, E. W. Meijer, and R. P. Sijbesma, Chem. Rev. (Washington, D.C.) **101**, 4071 (2001).
[3] *Molecular Recognition and Polymers; Control of Polymer Structure and Self Assembly*, edited by V. Rotello and S. Thayumanavan (Wiley, New York, 2008).
[4] M. Doi and S. F. Edwards, *The Theory of Polymer Dynamics* (Clarendon, Oxford, 1986).
[5] T. Annable, R. Buscall, R. Ettelaie, and D. Whittlestone, J. Rheol. **37**, 695 (1993).
[6] W. H. Binder and R. Zirbs, Adv. Polym. Sci. **207**, 1 (2007).
[7] F. Tanaka, Polym. J. **34**, 479 (2002).
[8] T. F. A. de Greef and E. W. Meijer, Nature (London) **453**, 171 (2008).
[9] P. Cordier, F. Tournilhac, C. Souile-Ziakovic, and L. Leibler, Nature (London) **451**, 977 (2008).
[10] W. B. Lee, R. Elliott, K. Katsov, and G. H. Fredrickson, Macromolecules **40**, 8445 (2007); R. Elliott and G. H. Fredrickson, J. Chem. Phys. **131**, 144906 (2009).
[11] M. Lísal, J. K. Brennan, and W. R. Smith, J. Chem. Phys. **130**, 104902 (2009).
[12] M. E. Cates, Macromolecules **20**, 2289 (1987).
[13] B. O'Shaughnessy and J. Yu, Phys. Rev. Lett. **74**, 4329 (1995).
[14] C.-C. Huang, H. Xu, J. Wittmer, and J.-P. Ryckaert, Lect. Notes Phys. **704**, 379 (2006); C.-C. Huang, H. Xu, and J.-P. Ryckaert, J. Chem. Phys. **125**, 094901 (2006).
[15] I. A. Nyrkova and A. N. Semenov, Europhys. Lett. **79**, 66007 (2007).
[16] E. B. Stukalin, J. F. Douglas, and K. F. Freed, J. Chem. Phys. **129**, 094901 (2008).
[17] It is impossible to cite all such studies; there have been very many. We focus on those most relevant to the current work.
[18] M. S. Green and A. V. Tobolsky, J. Chem. Phys. **14**, 80 (1946).
[19] M. E. Cates, Macromolecules **21**, 256 (1988).
[20] L. G. Baxandall, Macromolecules **22**, 1982 (1989).
[21] L. Leibler, M. Rubinstein, and R. H. Colby, Macromolecules **24**, 4701 (1991).
[22] F. Tanaka and S. F. Edwards, Macromolecules **25**, 1516 (1992); S.-Q. Wang, *ibid.* **25**, 7003 (1992).
[23] R. D. Groot, A. Bot, and W. G. M. Agterof, J. Chem. Phys. **104**, 9220 (1996).
[24] M. Rubinstein and A. N. Semenov, Macromolecules **31**, 1373 (1998); **31**, 1386 (1998).
[25] A. Vaccaro and G. Marruci, J. Non-Newtonian Fluid Mech. **92**, 261 (2000); R. J. J. Jongschaap, R. H. W. Wientjes, M. H. G. Duits, and J. Mellema, Macromolecules **34**, 1031 (2001).
[26] M. Rubinstein and A. N. Semenov, Macromolecules **34**, 1058 (2001).
[27] A. N. Semenov, Europhys. Lett. **76**, 1116 (2006).
[28] T. Indei, J. Chem. Phys. **127**, 144904 (2007).
[29] A. Semenov, A. Charlot, R. Auzely-Velty, and M. Rinaudo, Rheol. Acta **46**, 541 (2007).
[30] A. Tripathi, K. C. Tam, and G. H. McKinley, Macromolecules **39**, 1981 (2006).
[31] L. Pellens, R. G. Corrales, and J. Mewis, J. Rheol. **48**, 379 (2004); L. Pellens, K. H. Ahn, S. J. Lee, and J. Mewis, J. Non-Newtonian Fluid Mech. **121**, 87 (2004).
[32] J. Baschnagel and F. Varnik, J. Phys.: Condens. Matter **17**, R851 (2005).
[33] Notable exceptions are Refs. 20 and 27.
[34] S. K. Kumar, S. Shenogin, and R. H. Colby, Macromolecules **40**, 5759 (2007); W. Liu, D. Bedrov, S. K. Kumar, B. Veytsman, and R. H. Colby, Phys. Rev. Lett. **103**, 037801 (2009).
[35] K. E. Feldman, M. J. Kade, E. W. Meijer, C. J. Hawker and E. J. Kramer, Macromolecules **42**, 9072 (2009).
[36] R. D. Groot and W. G. M. Agterof, J. Chem. Phys. **100**, 1649 (1994).
[37] M. Nguyen-Misra and W. L. Mattice, Macromolecules **28**, 6976 (1995).
[38] Y. Liu and R. B. Pandey, J. Chem. Phys. **105**, 825 (1996).
[39] A. Milchev, J. P. Wittmer, and D. P. Landau, Eur. Phys. J. B **12**, 241 (1999).
[40] S. K. Kumar and J. F. Douglas, Phys. Rev. Lett. **87**, 188301 (2001).
[41] C. Ayyagari, D. Bedrov, and G. D. Smith, Polymer **45**, 4549 (2004).
[42] L. Guo and E. Luijten, J. Polym. Sci., Part B: Polym. Phys. **43**, 959 (2005).
[43] C. Manassero, G. Raos, and G. Allegra, J. Macromol. Sci., Phys. **44**, 855 (2005).
[44] S. M. Loverde, A. V. Ermoshkin, and M. O. de la Cruz, J. Polym. Sci., Part B: Polym. Phys. **43**, 796 (2005).
[45] F. Lo Verso, C. N. Likos, C. Mayer, and H. Löwen, Phys. Rev. Lett. **96**, 187802 (2006); F. Lo Verso, C. N. Likos, and H. Löwen, J. Phys. Chem. C **111**, 15803 (2007); F. Lo Verso and C. N. Likos, Polymer **49**, 1425 (2008).
[46] A. R. C. Baljon, D. Flynn, and D. Krawzsenek, J. Chem. Phys. **126**, 044907 (2007).
[47] M. Goswami, S. K. Kumar, A. Bhattacharya, and J. F. Douglas, Macromolecules **40**, 4113 (2007).
[48] K. Kremer and G. S. Grest, J. Chem. Phys. **92**, 5057 (1990).
[49] M. Rubinstein and R. Colby, *Polymer Physics* (Oxford University, New York, 2003).
[50] W. C. Yount, D. M. Loveless, and S. L. Craig, J. Am. Chem. Soc. **127**, 14488 (2005).
[51] D. M. Loveless, S. L. Jeon, and S. L. Craig, Macromolecules **38**, 10171 (2005).
[52] P. G. de Gennes, J. Chem. Phys. **76**, 3316 (1982); **76**, 3322 (1982).
[53] B. O'Shaughnessy, Phys. Rev. Lett. **59**, 2903 (1987); **71**, 3331 (1993).
[54] B. Friedman and B. O'Shaughnessy, Phys. Rev. Lett. **60**, 64 (1988).

[55] B. O'Shaughnessy and D. Vavylonis, Eur. Phys. J. B **6**, 363 (1998).

[56] G. H. Fredrickson and L. Leibler, Macromolecules **29**, 2674 (1996).

[57] W. C. Yount, H. Juwarker, and S. L. Craig, J. Am. Chem. Soc. **125**, 15302 (2003).

[58] D. Xu, J. Hawk, D. M. Loveless, S. L. Jeon, and S. L. Craig (unpublished).

[59] These experiments were largely performed with "floating" sticky monomers which can attach to any monomer on the parent chains, but since the SMs are bonded to at least one chain the vast majority of the time, for practical purposes the systems are APs as defined here.

[60] R. P. Sijbesma, F. H. Beijer, L. Brunsveld, B. J. B. Folmer, J. H. K. K. Hirschberg, R. F. M. Lange, J. K. L. Lowe, and E. W. Meijer, Science **278**, 1601 (1997).

[61] S. H. M. Söntjens, R. A. E. Renken, G. M. L. van Gemert, T. A. P. Engels, A. W. Bosman, H. M. Janssen, L. E. Govaert, and F. P. T. Baaijens, Macromolecules **41**, 5703 (2008).

[62] S. H. M. Söntjens, R. P. Sijbesma, M. H. P. van Genderen, and E. W. Meijer, J. Am. Chem. Soc. **122**, 7487 (2000).

[63] M. Pütz, K. Kremer, and G. S. Grest, Europhys. Lett. **49**, 735 (2000).

[64] G. S. Grest and K. Kremer, Macromolecules **23**, 4994 (1990); J. Phys. (France) **51**, 2829 (1990).

[65] R. Hentschke and E. Oyen, J. Chem. Phys. **122**, 104904 (2005).

[66] C. Svaneborg, R. Everaers, G. S. Grest, and J. G. Curro, Macromolecules **41**, 4920 (2008).

[67] J. Rottler and M. O. Robbins, Phys. Rev. E **68**, 011507 (2003).

[68] C. Bennemann, W. Paul, K. Binder, and B. Dünweg, Phys. Rev. E **57**, 843 (1998).

[69] S. Plimpton, J. Comput. Phys. **117**, 1 (1995); http://lammps.sandia.gov/

[70] D. Frenkel and B. Smit, *Understanding Molecular Simulations*, 2nd ed. (Academic, San Diego, 2002).

[71] For the NPT and deformation simulations we use a smaller timestep $\delta t = 0.008\tau_{LJ}$. For all simulations, because of the weak thermostatting and large timestep, we set a cap $0.075a\,\delta t$ on the maximum monomer displacement per timestep, to avoid crashes at large h. This restriction is rarely actively applied (the associated kinetic energy is $\sim 50k_BT$) and the need for it can be eliminated by using smaller δt.

[72] T. Schneider and E. Stoll, Phys. Rev. B **17**, 1302 (1978).

[73] C. Pastorino, T. Kreer, M. Müeller, and K. Binder, Phys. Rev. E **76**, 026706 (2007).

[74] R. Everaers, S. K. Sukumaran, G. S. Grest, C. Svaneborg, A. Sivasubramanian, and K. Kremer, Science **303**, 823 (2004).

[75] R. S. Hoy, K. Foteinopoulou, and M. Kröger, Phys. Rev. E **80**, 031803 (2009).

[76] R. Auhl, R. Everarers, G. S. Grest, K. Kremer, and S. J. Plimpton, J. Chem. Phys. **119**, 12718 (2003).

[77] K. Yamauchi, J. R. Lizotte, and T. E. Long, Macromolecules **36**, 1083 (2003).

[78] C.-C. Huang, H. Xu, and J. P. Ryckaert, Europhys. Lett. **81**, 58002 (2008); Phys. Rev. E **79**, 041501 (2009).

[79] The difference between $U_{sb}(r,h)$ and the potential used in Ref. 46 is that they absorbed the last two terms into a single offset U_{assoc}. The value $U_{assoc}=22u_0$ used in Ref. 46 corresponds to $h=4.1715u_0$.

[80] K. Esselink, L. D. J. C. Loyens, and B. Smit, Phys. Rev. E **51**, 1560 (1995).

[81] V. I. Manousiouthakis and M. W. Deem, J. Chem. Phys. **110**, 2753 (1999).

[82] Note that using a too-small τ_{MC} leads to effects similar to allowing SBs to break and reform during a single MC step; Huang et al. (Ref. 14) referred to such recombinations as "spurious." Rubinstein has pointed out that our algorithm produces changes in p^* for very fast kinetics ($\tau_{MC}\sim 0.01\tau_{LJ}$). This may be attributable either to a flaw in our MC algorithm or to physical "nonthermodynamic" effects of the type described in Ref. 93.

[83] S. K. Kumar and A. Z. Panagiotopoulos, Phys. Rev. Lett. **82**, 5060 (1999).

[84] S. Wang, C.-C. Chen, and E. F. Dormidontova, Soft Matter **4**, 2039 (2008).

[85] P. G. Khalatur, A. R. Khoklov, J. N. Kovalenko, and D. A. Mologin, J. Chem. Phys. **110**, 6039 (1999).

[86] J. T. Padding and E. S. Boek, Europhys. Lett. **66**, 756 (2004).

[87] M. Kröger, Phys. Rep. **390**, 453 (2004).

[88] M. Pitsikalis and N. Hadjichristidis, Macromolecules **28**, 3904 (1995); M. Pitsikalis, N. Hadjichristidis, and J. W. Mays, *ibid.* **29**, 179 (1996); D. Vlassopoulos, T. Pakula, G. Fytas, M. Pitsikalis, and N. Hadjichristidis, J. Chem. Phys. **111**, 1760 (1999).

[89] Except perhaps at high (processing) temperatures; for example, the variation in k_b with T for UPy in $CDCl_3$ (Ref. 62) indicates $h/k_BT \simeq 25$ for $T \simeq 300K$, so the same system at $T=450K$ would fall within our studied range of h/k_BT.

[90] G. D. Genesky, B. M. Aguilado-Mercado, D. M. Bhawe, F. A. Escobedo, and C. Cohen, Macromolecules **41**, 8231 (2008).

[91] I. Carmesin and K. Kremer, Macromolecules **21**, 2819 (1988).

[92] R. B. Pandey and D. P. Landau, J. Phys. A **18**, L399 (1985).

[93] E. Ben-Naim and P. L. Krapivsky, Phys. Rev. E **77**, 061132 (2008).

[94] A. Milchev, J. P. Wittmer, and D. P. Landau, Phys. Rev. E **61**, 2959 (2000).

[95] P. W. Atkins, *Physical Chemistry* (Oxford University Press, Oxford, 1978).

[96] C. Donati, S. C. Glotzer, P. H. Poole, W. Kob, and S. J. Plimpton, Phys. Rev. E **60**, 3107 (1999).

[97] A key difference is that the "cage" is typically much larger in an AP network well above T_g then it is in the same system near and below T_g; it is produced only by the sticky monomers in the former, but by all monomers in the latter.

[98] For $\tau_{MC}=\tau_{LJ}$. This value could in principle change as kinetics are slowed.

[99] This of course depends on the details of the shape and range of $U_{sb}(r)$. The effect of the form of the sticky bonding potential on AP dynamics is largely unexplored; to our knowledge, only Ref. 44 has examined the effects of varying the *range* of this potential.

[100] J. D. Ferry, *Viscoelastic Properties of Polymers* (Wiley, New York, 1980).

[101] This is valid for dense melts. If chains overlap less strongly, the dependence of a_{cage} on c_{st} can be different; see Ref. 24.

[102] For $h/k_BT \gtrsim 10$; at lower values, the single-exponential behavior of $P_{auto}(t)$ (Appendix B) gradually breaks down as h/k_BT decreases.

[103] Notable exceptions are Refs. 52, 55, and 56, but these considered the simpler case of irreversible SB formation. It would be interesting to see if these theories could be generalized to reversible AP networks.

[104] D. R. Rottach, J. G. Curro, J. Budzien, G. S. Grest, C. Svaneborg, and R. Everaers, Macromolecules **40**, 131 (2007).

[105] L. R. G. Treloar, *The Physics of Rubber Elasticity* (Clarendon, Oxford, 1975).

[106] E. M. Arruda and M. C. Boyce, J. Mech. Phys. Solids **41**, 389 (1993).

[107] Note that given that bond lifetimes are exponentially distributed rather than single-valued, it is not enough that $\tau_{sb} > \min(t_{cage}, t_{chem})$; it must be MUCH larger to reach the KL regime.

[108] Related effects were studied in simulations by Huang et al. (Refs. 14 and 78), but their systems of broadly polydisperse linear equilibrium polymers with $c_{st}=1$ are clearly different from both our monodisperse networks and dimeric systems with $c_{st} \ll 1$. The differences lie in the geometry of SM "caging" (or lack thereof).

[109] G. S. Grest, M. D. Lacasse, K. Kremer, and A. M. Gupta, J. Chem. Phys. **105**, 10583 (1996).

[110] H. A. Karimi-Varzaneh, P. Carbone, and F. Müller-Plathe J. Chem. Phys., **129**, 154904 (2008); Macromolecules **41**, 7211 (2008).

[111] J. Sprakel, J. van der Gucht, M. A. Cohen Stuart, and N. A. M. Besseling, Phys. Rev. Lett. **99**, 208301 (2007).

[112] S. Sen, Y. Xie, S. K. Kumar, H. Yang, A. Bansal, D. L. Ho, L. Hall, J. B. Hooper, and K. S. Schweizer, Phys. Rev. Lett. **98**, 128302 (2007).

[113] G. Allegra, G. Raos, and M. Vacatello, Prog. Polym. Sci. **33**, 683 (2008).

[114] P. G. de Gennes, *Scaling Concepts in Polymer Physics* (Cornell University, Ithaca, 1979).